INSIDER

Improved Nuclear SIte characterization for waste minimization in DD operations under constrained EnviRonment

Research and Innovation action
NFRP-2016-2017-1

Inventory of existing methodologies for constrained environments

Deliverable D5.1

Version no. 1

Authors: K. AMGAROU (CEA), M. HERRANZ (UPV-EHU), C. CSÖME (MTA-EK), F. ASPE (ONET)

http://www.insider-h2020.eu

Document Information

Grant Agreement #:	755554
Project Title:	Improved Nuclear SIte characterization for waste minimization in DD operations under constrained EnviRonment
Project Acronym:	INSIDER
Project Start Date:	01 June 2017
Related work package:	WP 5: In situ measurement
Related task(s):	Task 5.1: Review of state of the art in constrained environment
Lead Organisation:	CEA
Submission date:	31/01/18
Dissemination Level:	Public

History

Date	Submitted by	Reviewed by	Version (Notes)

Table of content

List of Tables

List of Figures

Summary

The INSIDER project aims at further improving the management of contaminated materials in nuclear facilities subject to a decommissioning programme, as well as during post-accidental site remediation and clearance, by proposing a methodology that allows the definition and selection of the most appropriate intervention scenarios producing well-characterized radioactive waste for which storage and disposal routes are clearly identified. To accomplish this, three strategic objectives have been outlined, the second of which is the "Performance assessment of available measurement techniques (methods and tools) to establish a science base for the decision-making". The first step of this second strategic objective is the validation of rapid and cost effective analytical methods (in lab and in-situ).

In this context, WP5 (in-situ measurements), which is in charge of the present deliverable, is devoted to the definition and implementation of practical considerations about in-situ radiological characterisation by means of non-destructive techniques. Activities carried out inside this work package are divided in different tasks. The second of these tasks involves making an inventory of available radiological characterisation methodologies, mainly in the fields of gamma-spectrometry, dose rate measurements and radiation imaging (gamma camera), which could potentially be applied in constrained environments in terms of radioactivity (medium or high radioactivity), under difficult accessibility conditions and/or in underwater interventions.

Hence, this first deliverable D5.1 contains a description of the main instruments used to establish the radiological situation of sites under D&D (decommissioning and dismantling) processes. This document describes instruments used for environmental radiation measurements (including dose rate monitors), surface contamination measurements, gamma spectrometry, neutron coincidence measurements, and radiation cameras. Although being exclusively an elemental analysis technique, laser induced breakdown spectroscopy (Radziemski & Cremers, 2006) can also be applied to provide complementary and useful information.

This deliverable does not claim to be exhaustive or a commercial catalogue of all the available technologies given that the basic principles of nuclear instrumentation and radiation detection are fully detailed in a number of text books and publications, most of which are referenced in this document's "Bibliography".

Most of the given information in this document will be of great support for future actions of the workpackage WP5, and it will be completed by two other reports. The first of them, deliverable D5.2, will be dedicated to the classification and categorisation of all the possible constrained environments and the final one, deliverable D5.3, will consist of a collection of recommended in-situ measurement techniques for each constrained environment. This last document will connect the techniques and tools described in the present deliverable D5.1 to the constrained environments described in deliverable D5.2. Thus, these three deliverables should be considered as a whole.

To check the ability of some specific equipment and associated software, belonging to those techniques described in deliverable D5.1, in-situ measurement campaigns will be carried out under

different constrained environments, called use cases. The challenge in these campaigns is not only the identification of the most appropriated use cases, task under the responsibility of work package 2, but also to find at least three participants working with the same topic, although using different equipment and software. Results of such campaigns will allow to validate all the techniques used as well as the recommendations formulated in deliverable D5.3.

Among the different tasks carried out by this work package WP5, this one is of key importance as it is the first time that benchmarking campaigns is planned for in-situ measurements of nuclear facilities subject to a decommissioning programme.

1   Introduction

In line with the general objectives of the INSIDER project, the work package WP5 is devoted to the definition and implementation of practical considerations about in-situ radiological characterisation of nuclear facilities subject to a decommissioning programme, taking into account specific outputs from WP2, WP3 and WP4.

Such an activity is mainly based on non-destructive assay methods to detect all types of ionizing radiation emitted by radionuclides such as helium nuclei (α), electrons (β^-), positrons (β^+), energetic photons (X- or γ-rays) and neutrons, without affecting the physical or chemical form of the item under examination.

The simplest, fastest and most inexpensive method that can be used is the one based on measuring the radiation levels at predetermined locations to map the associated spatial distribution or cartography of wide-areas (Mikami et al., 2015). The corresponding results serve to localize the potential presence of radioactive singularities or hotspots, and can be roughly correlated with the activities of the major gamma emitting radionuclides, thus allowing a first screening of contaminated areas.

Although this method is widely applied, it is seriously affected by uncertainties in the measurement geometry, in the own characteristics of the measurement probe used and in the environment parameters to be considered. In addition, cartography of alpha/beta contamination on surfaces would be of great utility (Leskinen et al., 2013).

Other sophisticated methods that can be applied for in-situ measurements are gamma spectrometry, passive neutron counting, and radiation cameras (Amgarou et al., 2016; Baschenko, 2004; Cieślak, 2016; Gal et al., 2001; Knoll, 2010; Lamadie et al., 2005; Reilly et al., 1991; Woolf et al., 2015; Takeda et al., 2012). Although being exclusively an elemental analysis technique, laser induced breakdown spectroscopy (Radziemski & Cremers, 2006) can also be applied to provide complementary and useful information.

Certain nuclear facilities, or some of their components, contain complex or non-standard infrastructures with limited accessibility and intense radiation fields. For such constrained environments, new methodologies are necessary for a more accurate initial estimation of the radioactive source term. These will be based on advanced statistical processing and modelling, coupled with adapted and innovative analytical and measurement methods, which take into account sustainability and economic objectives. Robotics or other remotely deployed systems based on reduced-size detectors are a good alternative, but collimation mechanisms with small opening angles may also be considered to restrict the field-of-view of the chosen instruments to only specific areas or portions of the item to be measured. The acquisition is then performed at different positions around the object providing a high degree of precision.

Radiation measurement techniques that are commonly used for in-situ radiological characterisation of nuclear facilities are broadly discussed throughout the rest of this document. Although some basic concepts are assumed, the interested reader is referred to Knoll (2010), Reilly et al. (1991) and Tsoulfanidis & Lansberger (2015) for more details about the nuclear instrumentation and radiation detection.

2   Environmental radiation measurements

At any nuclear facility, environmental radiation measurements are generally conducted at different positions around its structures and equipment in order to investigate their radiological status, to evaluate the effectiveness of protection measures, as well as to assess the associated doses likely to be received by individuals. This is also true before, during and at the end of dismantling activities. Depending on the type of information provided, the different measurement techniques used in this domain can be classified into the following three groups: gross counting counters, air-kerma[1] monitors and probes measuring the ambient dose equivalent or $H*(10)$.

2.1   Gross counting counters

Gross counting instruments are primarily used to detect the presence of radioactive material, and the most commonly used one is the Geiger-Müller (GM) counter, which consists of a gas-filled tube usually containing 98% helium and 1.3% butane at a low pressure (~0.1 atmosphere). The walls of the tube are either made of metal or have their inner surface coated with a conducting material or a spiral wire to operate as a cathode, whereas the anode is made of a wire mounted axially in the centre of the tube. By applying a potential difference of several hundred volts, each incident ionizing radiation is able to produce a detectable electronic "pulse" or "count" through both the gas multiplication and electron avalanche mechanisms (Knoll, 2010).

The main advantage of GM counters is that they are cheap and robust with a large variety of sizes, requiring minimal electronic processing. However, as almost all generated pulses have the same height, regardless of the number of original ion pairs that initiated the process, these detectors cannot distinguish between radiation types or energies, and they are not able to measure high dose rates due to their excessive dead time (~100 μs). In addition, sustained high radiation levels will definitively degrade their detection performance, so they are not recommended for constrained environments.

In some medical applications, GM counters can be used to measure the integrated exposure[2], as long as the energy of the X- or γ-rays is well known and the instrument is calibrated for this particular energy. At best, for a given photon energy, the count rate (i.e., number of count per unit time) will respond linearly with the intensity of the radiation beam. However, for most nuclear facilities, the presence of several radioactive sources emitting X- or γ-rays at various energies will necessary result in erroneous and unreliable readings.

2.2   Air-kerma monitors

In general, direct measurement of the kerma quantity, the definition of which is given in Appendix A, is not possible. Air-kerma is universally determined by measuring the amount of ionization produced

---

[1] Kerma is an acronym for *"Kinetic Energy Released per unit Mass"*. The final *"a"* being added principally to avoid confusion with the German word *"kern"*, which means nucleus.

[2] Radiation exposure is defined as the electric charge per unit mass created by an incident radiation in a specified volume of dry air. Its legacy unit is called Roentgen or R (1 R = 1 0.000258 C/kg).

in air by an incident radiation and ionization chambers[3], which are the reference instruments for this purpose. These chambers have a good response to photons, which is uniform over a wide range of incidence energies, as well as less dead time effect (1 – 10 µs), and can also tolerate intense radiation fields (up to 10 Gy/h).

An ionization chamber consists of a gas-filled tube at atmospheric pressure which, contrary to a GM counter, operates at a very low electric field strength to avoid both the gas multiplication and electron avalanche mechanisms[4]. Under such circumstances, when an ionizing radiation interacts with the gas molecules, it generates electron-ion pairs along its path. The generated ions then drift to the cathode under the influence of the electric field whilst free electrons are collected by the anode, and the resulting current remains constant over a given range of the applied voltage.

However, ionization chambers used as air-kerma monitors cannot discriminate between radiation types and cannot provide the corresponding energy spectrum. Their wall material is normally selected to have an effective atomic number similar to that of air ($Z_{eff} = 7$ according to Tahmasebi Birgani et al., 2012). This "*air equivalent*" material has the effect of ensuring that the whole detector acts as an infinite air volume to reach an electronic equilibrium and an accurate ionization measurement. The electric field also enables the device to work continuously by mopping up electrons, which prevents both the fill gas from becoming saturated, where no more ionization could be collected, as well as the recombination of electron-ion pairs, which would diminish the registered current. This mode of operation is referred to as "current" mode, meaning that the output signal is a continuous current, and not a pulse output as in the cases of the Geiger-Müller tubes or the proportional counters.

Another alternative to measure air-kerma in the case of energetic photons is the one based on the energy-compensated silicon diodes (Ören et al., 2016). Compared to air, these detectors have the inherent advantages of a low ionisation energy and high density, thus allowing very small-sized detectors to be used for routine surveys in nuclear facilities. Nevertheless, it must be pointed out that air-kerma measurements are not trivial and must always consider several correction factors, namely the ones associated to the possible variations with respect to the environmental parameters (air pressure, temperature and humidity) under which the detector calibration was carried out.

2.3   H*(10) probes

As explained in Appendix A, the ambient dose equivalent is an imaginary quantity commonly used for monitoring strongly penetrating ionizing radiation, such energetic photons and neutrons, as a proxy of the effective dose, **E**, which can never be measured in realistic situations because it requires knowing the doses delivered to all organs and tissues in the human body.

2.3.1   The case of X- or γ-rays

As illustrated in Figure 1, the ambient dose equivalent in the case of X- and γ-rays is very conservative, from a radiation protection point of view, since it generally overestimates the effective

---

[3] In fact, ionization chambers are primarily suited to directly measure the radiation exposure, which is proportional to the corresponding energy released by the incident radiation in the considered air volume, so that a conversion factor can be used to convert between air-kerma and exposure values.
[4] A gas-filled tube can operate under different modes by only varying the applied voltage (Knoll, 2010).

dose to around 15% - 50% along the energy range of interest (50 keV – 2 MeV). However, it can even exceed a factor 2 for low energy photons.
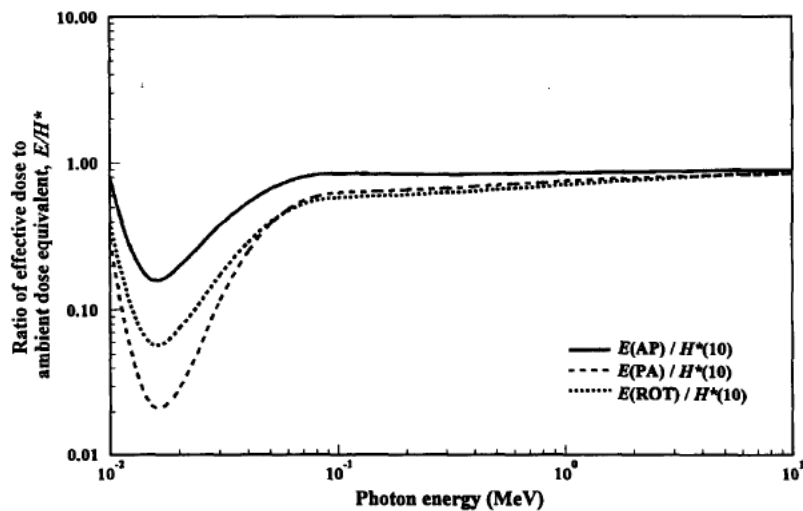
Figure 1: Ratio between the ambient dose equivalent, $H^*(10)$, and the effective dose, E, as a function of the photon energy for various irradiation geometry: anterior–posterior (AP), posterior–anterior (PA) and rotational (ROT) (ICRP, 1996).

Practically any type of photon detector is able to measure $H^*(10)$, but the preferable one is that consisting of a proportional counter, which is a gas-filled tube operating in a voltage region immediately after that of an ionization chamber. Consequently, the electric field strength is intense enough to accelerate the original free electrons generated by the incident radiation to energies so high that their collisions with the gas molecules cause further ionizations. This effect, called gas multiplication (Knoll, 2010), makes the height of the output electric pulse proportional to the energy deposited by the incident radiation. Hence, a proportional counter is able to discriminate between radiation types and to provide the corresponding spectrometric information. By employing a noble gas, such as Xenon or Krypton, and even increasing its associated pressure, the photon detection efficiency can be considerably enhanced. Like ionization chambers, proportional counters have a small dead time effect (1 – 10 μs) and they can tolerate high radiation levels.

The chosen measurement instrument needs to be properly calibrated using standard radioactive sources (most often ^{137}Cs) and considering a free-air geometry configuration (i.e. both the source and the detector are suspended in air within a large room). Hence, for the chosen source-to-detector distance with known $H^*(10)$ value, the associated reading M is obtained, and the corresponding calibration factor is simply determined as:

$$\text{CF} = \frac{H^*(10)}{M}$$

2.3.2 The case of neutrons

The problematic is extremely complex in the presence of neutrons, as their energy spectrum may cover, at the same time, a total of 10 decades ranging from thermal[5] to around 20 MeV, and they do not produce primary ionization when passing through matter, due to their lack of Coulomb interactions with the surrounding atoms and molecules. The sole way to detect them is through the secondary charged particles released from their nuclear interactions in the considered medium. Consequently, the neutron detection imperatively needs the addition of a converter material offering a significant interaction likelihood to produce this desired ionization process. The most commonly used are ^{3}He, ^{6}Li or ^{10}B due to their optimum cross-section for thermal neutrons, as shown in Figure 2. To detect more energetic neutrons, both the detector and converter are normally surrounded by an additional moderating material, made of polyethylene, so that the energy of incidence is previously slowed down via multiple and/or successive elastic collisions with Hydrogen nuclei. In most cases, further refinements are needed in terms of associated electronics to differentiate between the neutron-induced pulses from those that may be generated by the gamma radiation. Table 1 summarizes the strengths and weaknesses of the most common neutron detectors.
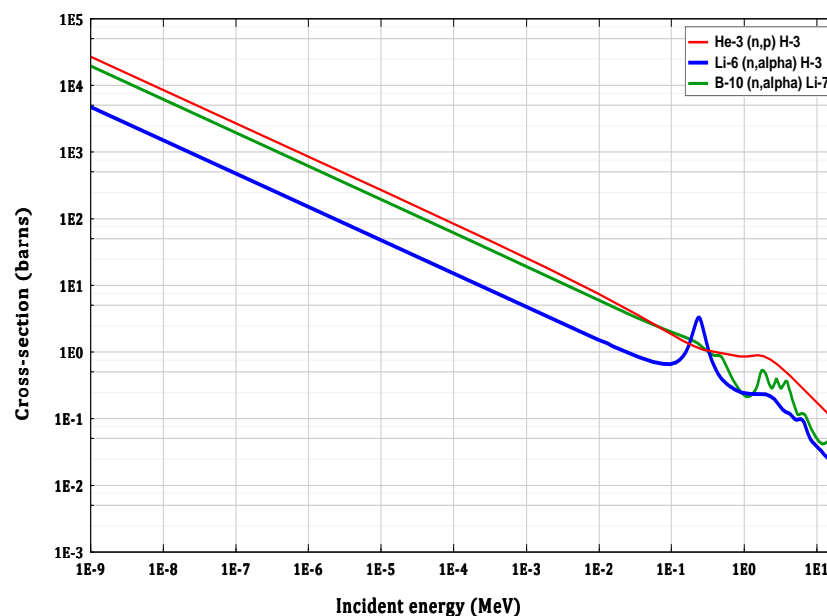
Figure 2 : Cross-section vs. incidence energy for some nuclear reaction of interest in neutron detection (Source: JANIS[6]).

However, independently of the considered configuration of the detector itself, the converter material and the moderator, satisfactory results in terms of the neutron ambient dose equivalent are only obtained in restricted energy intervals and/or in specific irradiation conditions. Therefore, the chosen instrument must be previously calibrated under the same experimental configurations or at least considering a representative neutron spectrum (IAEA, 2001). Another possibility to properly estimate $H^*(10)$ would be the preliminary determination of the spectrometric information about all the possible neutron fields in order to derive the proper transfer function for each location. Among several

---

[5] Neutrons with energies between 1 meV and 1 eV.
[6] Available at: https://www.oecd-nea.org/janis/

complex neutron spectrometry techniques, only the well-known Bonner sphere system (Bramblett et al., 1960) is able to measure neutron spectra, independently of their direction of incidence, over the whole energy range of interest (i.e., 10^{-3} eV – 20 MeV). The system consists of a set of polyethylene multi-sphere moderators of various sizes (typically labelled in inches between 2" and 12"), surrounding a central detector that is mostly sensitive to thermal neutrons. As the size of the sphere increases, the maximum response of the sphere-detector combination shifts to the highest neutron energies (see Figure 3). To derive the spectral contribution of thermal neutrons, an additional measurement must be performed using the central detector in bare configuration or by adding a thin (1mm) cadmium shell to the smallest sphere.

Table 1: Strengths and weaknesses of the most common neutron detectors (Knoll, 2010).

Detector type	Strengths	Weaknesses
^{3}He proportional counter	Reasonably light Good neutron cross-section High filling pressure Resistant to intense radiation fields	Reduced γ pulse discrimination Sensitive to movement vibration ^{3}He shortage
BF$_3$[7] proportional counter	Reasonably light Good γ pulse discrimination More readily available than ^{3}He Resistant to intense radiation fields	Low neutron cross-section Sensitive to movement vibration Limited filling pressure Toxic and corrosive
LiI(Eu) scintillator[8]	Compact design Detection efficiency[9] Insensitive to movement vibration	Reduced γ pulse discrimination Hygroscopic material Pile-up effect
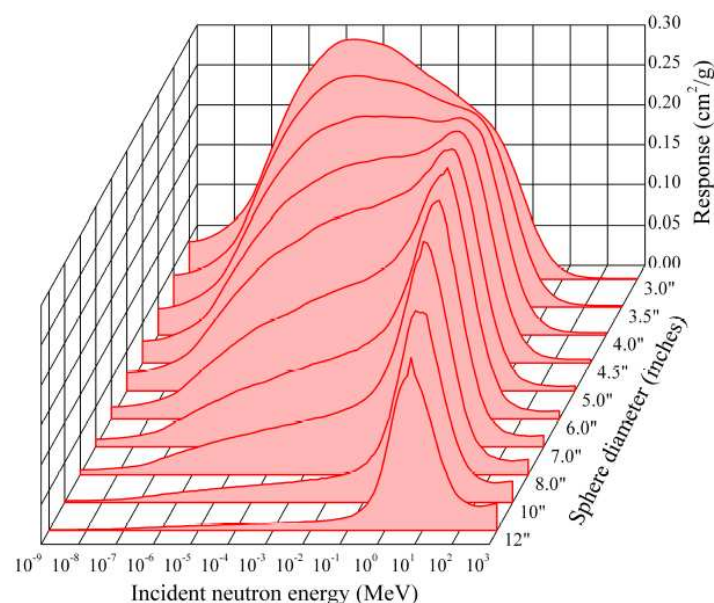
Figure 3: Response functions of a Bonner sphere system (Amgarou & Lacoste, 2010).

---

[7] Boron trifluoride.

[8] Europium-activated lithium iodide.

[9] The high density of the crystal fully compensate for the very low cross-section of ^{6}Li (see Figure 2).

3   Surface contamination measurements

Surface contamination can be *"fixed"* or *"removable"*. *"Fixed"* contamination is that which is not transferred from a contaminated surface to an uncontaminated one when they accidentally touch; conversely, *"removable"* contamination (sometimes called *"loose"* contamination) is that which may be readily transferred under the same circumstances.

Surface contamination measurements should provide a quantitative analysis of activity per unit area of the radionuclides present in the surface. However, without previous knowledge of the radionuclides and processes responsible for a surface contamination, it is not always possible to carry out such a quantitative analysis. Specific instruments designed for this purpose should be used but in most cases, they will only be able to provide a qualitative comparison with clean surfaces and an assessment of which part of the contamination is fixed. In this situation, calibration is not a challenge for these techniques.

In cases when contamination can be clearly characterized, complex radionuclide-specific calibrations of the measurement equipment are required. Some guides on how to carry out these calibrations can be obtained from ISO standard 7503.

In any case, contamination can be measured by direct methods, which measure the amount of fixed and removable contamination directly from the contaminated surface using surface contamination instruments, or by indirect or smearing methods, which only measure removable contamination, from a sample taken from the contaminated surface using a wipe test. The collected wipes can be measured directly in a counter and/or can be sent to a radiochemical laboratory for more precise analysis. This particular topic is the core of the work package WP4 in the INSIDER project.

Both direct and indirect methods need to be adapted to account for technical issues. Several aspects must be considered before choosing between direct or indirect methods. Direct measurements should be used in accessible surfaces free of solid or liquid deposits and in absence of radiation fields that may interfere with the equipment. When these conditions are not met, indirect methods should be used, despite the fact that they cannot assess fixed contamination and they have a high uncertainty because of the lack of knowledge of the wiping efficiency.

Table 2 provides an overview summarizing the strengths and weaknesses of each method. In many circumstances, the two methods are complementary and both should be used to achieve a complete assessment of the state of the zone under study.

Table 2: Strengths and weaknesses of surface contamination measurements.

Method type	Strengths	Weaknesses
Direct	Total contamination measurement Large areas control	Gamma radiation interference
Indirect or smearing	No gamma radiation interference Access to removable contamination	Wiping efficiency Fixed contamination representability

The radiation detector needs to be as close as possible (~1cm) to the object under examination and the person responsible for conducting this kind of measurement must be extremely careful not to

contaminate the detector itself. Yet again, proportional counters are the preferred measurement instruments for this purpose because they offer the possibility to distinguish between alpha and beta particles and to design large, flat detection areas that range from 50 cm^2 up to 1000 cm^2. The two cases relating to alpha and beta contaminations are discussed separately below.

3.1 Alpha contamination

Because of the extremely low penetration of alpha particles, special techniques must be used to allow the particles to enter the active region of a detector, while simultaneously protecting this active region. Most times, an ultra-thin window, for radiation entrance, made of an aluminized Mylar or mica film ($\sim 2 \times 10^{-3}$ g/cm^2) is used; thus, contact with any hard object may puncture it. This can cause a gas exhaust in the case of proportional counters, or the entrance of ambient light to sensitive crystal in the case of scintillators detectors, hence overwhelming the photomultiplier tube. When it comes to alpha detectors, the requirement that they must be as close as possible to the object under examination without ever touching it makes direct methods impractical, except in special and controlled situations (e.g. monitoring individuals at the hot line or air sampler filters).

3.2 Beta contamination

Most of the problems that can be encountered during the measurement of alpha contamination do not apply for β-particles due to their relatively high penetrating power, allowing the increase of end-window thickness. However, as they are not mono-energetic, their identification on the basis of energy resolution is virtually impossible. In principle, as most of these detectors are also sensitive to gamma radiation, they cannot distinguish the individual contribution of each one of them. One solution could be simply to vary the source-to-detector distance, or to use an appropriate filter to prevent any emitted β-particle to reach the sensitive volume of the detector, thus enabling a gamma-only measurement to be made.

4 Gamma spectrometry

Gamma spectrometry is the start technique for in-situ measurements, as most of the radionuclides emit characteristic X-ray and gamma radiation with specific energies and intensities, making their identification and even their quantification possible (Pérot et al., 2018). Its general principle consists in measuring these mono-energetic photons by a detector which delivers a signal that is proportional to the absorbed energy within the sensitive volume. This signal is then analysed and classified in the form of a histogram commonly known as a "*gamma spectrum*" (see Figure 4). The usage of a multi-channel analyser (MCA) and evaluation algorithm is henceforth recommended.

Ideally, when an incident photon deposits all its energy in the detector, a very narrow peak should appear on the spectrum. But in practice, this peak is broadened due to the statistical fluctuations in the detection process and the noise added by the associated electronics. This widening, called energy resolution, mainly depends on the measurement instrument used and reflects its ability to separate different gamma emitting isotopes at neighbouring energies.
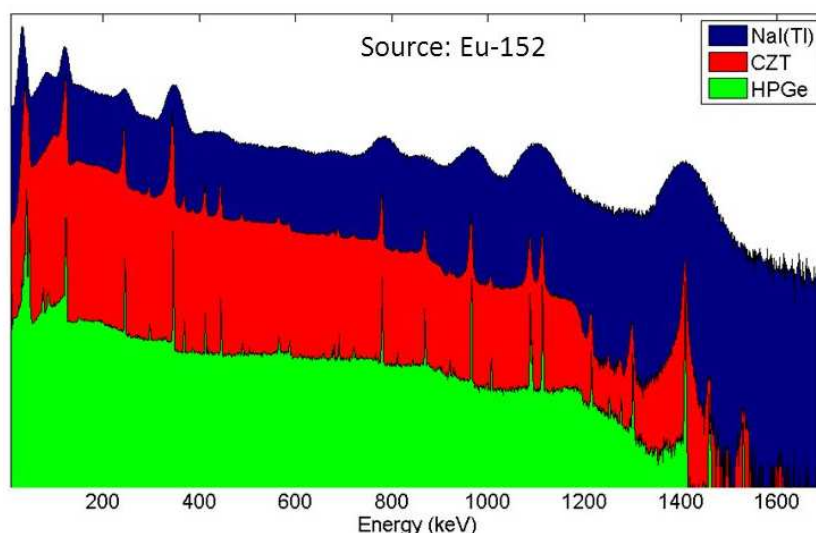
Figure 4: Pulse-height distributions for the same [152]E source as measured by different detectors.

Another parameter to be taken into account for quantitative measurements is the absolute detection efficiency[10], making possible the connection between the net area under the observed peak on the spectrum and the corresponding activity of the radioelement. It depends on the type of detector selected (material, density, sensitive volume, associated electronic, etc.), the energy of gamma radiation, the considered geometric configuration (measurement distances, use of collimation, shielding, screens, etc.), as well as the corresponding self-attenuation processes in the measured item. A complete characterisation of the detector response is normally carried out by means of radioactive standard sources and numerical simulations using the well-known MCNPX code (Pelowitz, 2011).

When using gamma spectrometry for in-situ measurements, the measured net count rates under the observed peaks are converted into activity concentrations (typically in units of Bq/kg or Bq/cm^3) of the associated radionuclides, taking into account several hypotheses regarding the spatial distribution of the radioactive source term within the object under examination (IAEA, 2017). For this purpose, as nuclear facilities contain huge and complex equipment, *ad hoc* transfer functions are calculated on a case-by-case basis from a theoretical model representing the physical characteristics of the object itself (shape, geometry, material composition, density, etc.), the different measurement distances, and all the possible spatial distributions of the sought radionuclides.

The gamma spectrometers most commonly employed for in-situ measurements are based on inorganic scintillators, such as NaI or LaBr, as well as on high-purity germanium (HPGe), CdTe or CdZnTe semiconductors. Their typical energy resolutions are summarized in Table 3.

---

[10] By definition, the absolute detection efficiency of a given radiation detector is the number of recorded pulses or counts divided by the number of ionizing particles emitted by the measured radioactive source, whereas the intrinsic detection efficiency is the same number of recorded pulses or counts but divided by the number of incident ionizing particles.

Table 3: Typical energy resolution for different gamma spectrometers.

Energy	NaI	LaBr	CdZnTe	CdTe	HPGe
122 keV	~15 keV	~8 keV	~8 keV	~2 keV	~0.5 keV
662 keV	~50 keV	~20 keV	~20 keV	~4 keV	~1.3 keV

All these spectrometers are usually used under an open geometry, also known as *"one shot"* measurement, with the detector located in a fixed position allowing it to "*see*" the whole volume of the object to be measured. However, the corresponding results are generally more sensitive to the variations in the radioactivity distribution within objects and their matrix effect. As stated in the introduction, a collimation mechanism with a small opening angle can be added to the detector to reduce the associated uncertainties (see Figure 5).

Figure 5: Measurement of a vessel containing radioactive effluents with a collimated HPGe detector (Pérot et al., 2018).

The gamma spectrometry technique is very limited by the attenuation of the radiation in the material. For very dense materials (e.g. concrete of 2 to 3 g/cm^3 density), the measurable depth of matrix is only a few dozen centimetres for the gamma emissions of the major radioactive isotopes (50 keV to 2 MeV). In some instances, the concrete waste must be broken up and measured in small baskets before it is placed in a large volume container (between 1 and 10 m^3).

4.1 Scintillation detectors

Scintillation is the emission of a flash of light in transparent materials by the passage of ionizing radiation. A scintillation detector is obtained when a scintillator crystal (NaI, CsI, SrI$_2$, LiI, LiF, LaBr$_3$, LaCl$_3$, CeBr$_3$ etc.) is coupled to an electronic light sensor, traditionally a photomultiplier tube (PMT). PMT absorbs the light emitted by the scintillator and re-emits it in the form of electrons (photo-electrons) via the photoelectric effect. From the multiplication of the electrons in the PMT, an electrical pulse that provides meaningful information about the energy deposited by the incident radiation can then be obtained and analysed.

Scintillation detectors can be manufactured in large volumes, but they generally have poor energy resolution. They are therefore often used for low intensity photon flux measurements with simple gamma spectra. However, since most scintillators have a very fast signal response (of the order of nanoseconds), they can also be used at high counting rates or for coincidence counting.

4.1.1 NaI(Tl)

Sodium iodide crystal activated with thallium or NaI(Tl) is the oldest and most widely used scintillator material to perform gamma spectrometry. It has a very high detection efficiency and is available in a wide variety of sizes and geometries. However, its energy resolution is very limited (typically around 7% at 662 keV), it does not tolerate high radiation levels (see Figure 6) and it is hygroscopic. Consequently, it cannot tolerate exposure to humid environments and it requires the use of a hermetically sealed assembly, which can hinder the detection efficiency for low gamma energies. The detector encapsulation is often made from low atomic number metal or metal alloys (e.g. aluminium, copper-aluminium). This detector provides a stable energy resolution and constant decay time of the light pulses over a wide range of temperatures (from -30 ℃ to 60 ℃, according to Moszynsky et al., 2006). It can also be used in underwater applications inside a nuclear fuel storage pool for real-time monitoring.
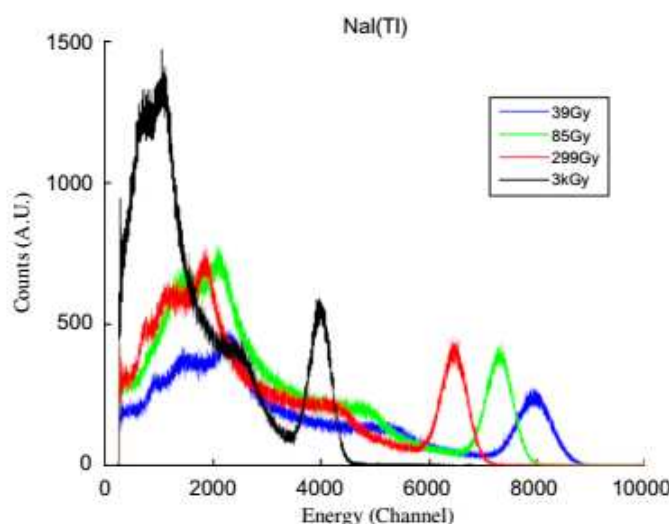
Figure 6: Cs-137 spectra as measured by a NaI(Tl) detector for various cumulative dose (Normand et al., 2006).

4.1.2 LaBr

Cerium-doped lanthanum bromide or $LaBr_3(Ce)$ scintillation detectors, most often referred to as "*LaBr*", offer improved energy resolution (around 3% at 662 keV) compared to NaI(Tl). This improved resolution is due to a light yield that is 160% greater than that achieved with sodium iodide. It also provides fast emission rates and excellent temperature tolerance (Bizarri et al., 2006), as well as good resistance to intense radiation fields (see Figure 7). Although the LaBr crystals are currently available in small sizes, they are very appropriate for constrained environments, together with silicon drift detectors (SDD) and silicon photomultipliers (SiPM).
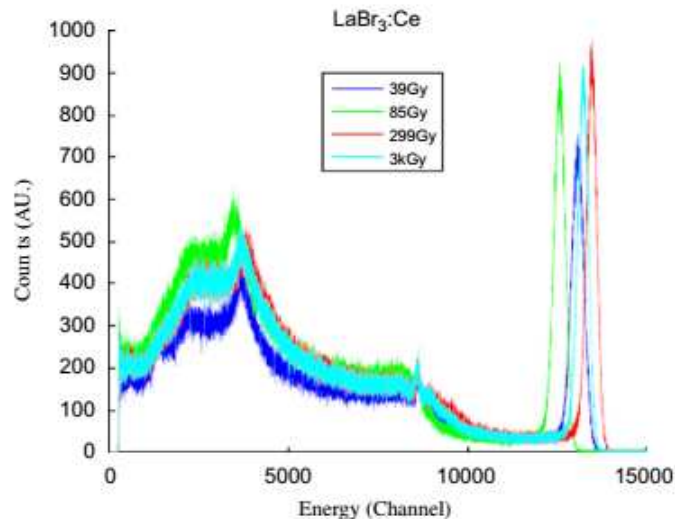
Figure 7: Cs-137 spectra as measured by a LaBr₃(Ce) detector for various cumulative doses (Normand et al., 2006).

4.2   Semiconductor detectors

In semiconductor detectors, ionizing radiation is measured by the number of charge carriers set free by the radiation in the substrate material (usually germanium, silicon, CdTe, CdZnTe, etc.), which is arranged between two electrodes. Under the influence of an electric field, the number of collected charge carriers (electrons and holes) is expected to be proportional to the amount of energy deposited by the passage of ionizing radiation, resulting in an electric pulse that is significantly lower than in scintillation detectors, but also has less statistical variation and better energy resolution. Their detection efficiency is often quoted in relative terms to that of a $3'' \times 3''$ NaI(Tl) scintillation detector.

It must be highlighted that semiconductor detectors are relatively sensitive to performance degradation when exposed to intense radiation fields, namely the ones containing neutrons. Electronic components are also radiation-sensitive, particularly the preamplifiers, which are the first stage in the signal processing chain for most scintillators and semiconductor detectors.

4.2.1   HPGe detectors

The operating principle of germanium detectors is fully based on that of a *p-n* junction, which is a microscopic zone, depleted of charge carriers, created in the contact between an *n*-type semiconductor (i.e. with an excess of free electrons) and a *p*-type semiconductor (i.e. with an excess of free holes) from the same crystal. This junction behaves like a diode, allowing the electric current to flow only in one direction, and can be expanded high enough for the detection of both X- and γ-rays, under a reverse-biased[11] voltage.

---

[11] Bias is the application of a voltage across a *p-n* junction; forward bias is in the direction of easy current flow, and reverse bias is in the direction of no current flow.

However, without purification techniques, Ge crystals cannot be employed as gamma spectrometers. Indeed, impurities in the crystal material trap electrons and holes that may be generated by the incident radiation, ruining the performance of the detector.

High-purity Germanium (HPGe) detectors are characterised by an excellent energy resolution, which makes it possible for them to distinguish the numerous X- and γ-rays emitted by radionuclides. In addition, they may have large sensitive volumes, ranging from cm^3 to about 1 litre, allowing the total absorption of photons up to several MeV.

Their major drawback is that the crystal must be placed in a vacuum cryostat and must be cooled to liquid nitrogen temperatures, which limits their usefulness in a number of applications, namely in zones with limited accessibility.

In environments where the electronics can be damaged by the circumstances (e.g. intense radiation fields), it is possible to use a low-noise charge preamplifier allowing the remote control from large distances of the detector with adequate shielding (Pullia et al., 2005). However, despite this solution, the Ge crystal itself still remains very sensitive to highly irradiating environments.

4.2.2   CdTe and CZT detectors

Cadmium telluride (CdTe) and cadmium zinc telluride (CdZnTe or CZT) crystals belong to the same family of compound semiconductors. Their main advantage, when compared to the HPGe ones, is their high detection efficiency, as a result of their high atomic number and density, which favours photoelectric interactions, as well as a wide band gap[12] that allows them to operate at room temperatures (i.e. from -5 °C to 50 °C, according t o Park et al., 2010) without requiring liquid nitrogen or electrical cooling.

Their energy resolution is not as optimal as that of HPGe, but it is slightly better than that of scintillators. In contrast, they are characterized by a poor mobility for both electrons and holes due to the charge trapping effect caused mainly by structural defects, impurities and other irregularities (e.g. dislocations, inclusions). This usually results in the so called low-energy tailing of the observed peaks in the measured spectrum.

CdTe and CZT detectors are generally fabricated with *ohmic* or *Schottky* contacts[13], allowing in-situ measurements over a wide range of radiation levels between 10 µGy/h and 100 mGy/h. The corresponding radiation-induced damage has been investigated by Cavallini et al. (2001), demonstrating that CdTe was quite insensitive to a commutative ^{60}Co gamma dose up to 10 kGy, while exposure above this value would cause a complete degradation in terms of spectroscopic capabilities, such as a loss of energy resolution and an incomplete charge collection (see Figure 8). On the other hand, CZT started degrading only after 25 kGy irradiation (see Figure 9).

---

[12] A band gap is a separation in terms of energy between valence band and the conduction band.
[13] An ohmic contact is a metal-semiconductor-metal (MSM) configuration allowing the electric current to flow in both directions in a similar way as a resistor (hence the name "ohmic"), whereas a Schottky contact only allows the current to flow in one direction, like a diode.
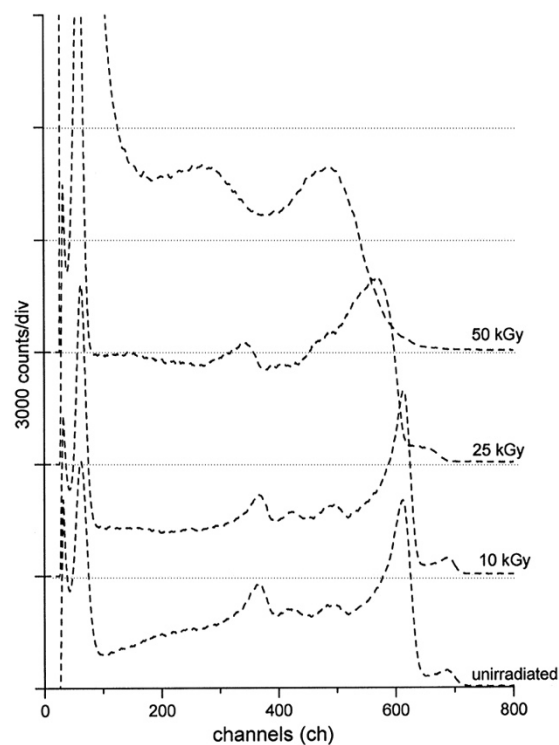
Figure 8: [57]Co spectra acquired by a CdTe detector before and after successive exposure to a ^{60}Co irradiator (Cavallini et al., 2001).
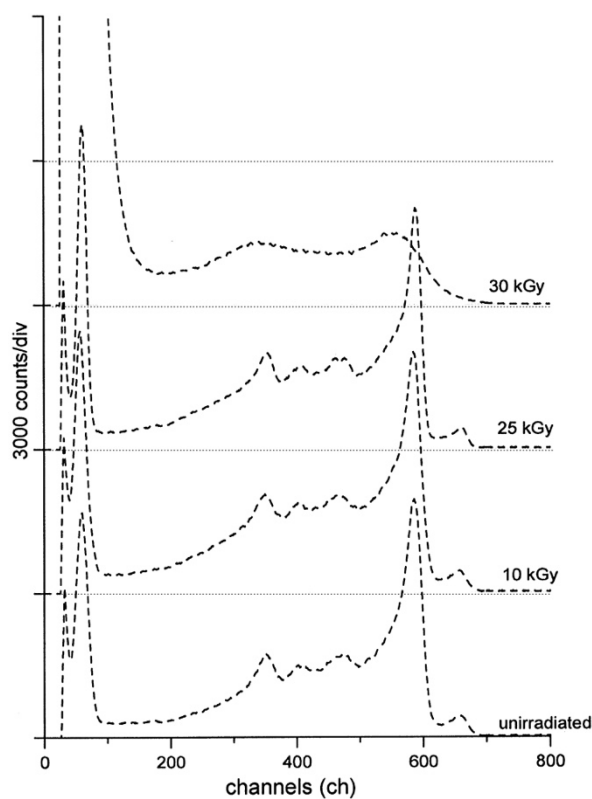
Figure 9: [57]Co spectra acquired by a CZT detector before and after successive exposure to a ^{60}Co irradiator (Cavallini et al., 2001).

5   Neutron coincidence measurements

Passive neutron measurement (Ensslin et al., 1998), using portable systems like the one developed by ORTEC[14], is another non-intrusive characterisation method that may provide relevant information about the presence of fission materials in the considered items through the analysis of the spontaneous neutrons emitted by the following plutonium isotopes: ^{238}Pu, ^{240}Pu and ^{242}Pu (Pérot et al., 2018).

The main advantage of this method is its relatively low sensitivity to the density of materials surrounding the radioactive elements. Compared to gamma spectrometry, it is practically insensitive to metallic matrices, commonly found in radioactive waste measurements, making these two techniques quite complementary.

However, passive neutron measurement is extremely affected by a number of frequently unknown – or incompletely known – properties, such as the presence in the sample of ^{242}Cm and ^{244}Cm, as the spontaneous neutron emission from these radionuclides is particularly intense, representing a factor of around 4170-20600 times higher than for the plutonium isotopes (see Table 4). In addition, (α,n) reactions, especially in the case of short-term actinides (see Table 5), are able to produce a single fast neutron following the interaction of their α particle emitted during their disintegration with a light element present in the medium, such as Be, B, C, O, F, etc. The presence of materials rich in hydrogen may also may reduce the signals of interest.

In its basic mode of application, the passive neutron measurement aims to detect all neutrons, without distinction of emission process: it is the total neutron counting. Depending on the application, ^{3}He or boron-coated proportional counters, as well as fission chambers and liquid or plastic scintillators, are used. However, this approach has the disadvantage of having a high sensitivity to the chemical form of the radioactive contaminant (metallic, oxide, or fluorinated plutonium, americium, or other actinides) via its (α,n) component for which neutron production can vary by a factor of up to 1100 with the nature of the light element (see Table 6).

To compensate for this disadvantage, it is necessary to discriminate the signal fraction originating from the spontaneous fissions from that resulting from (α,n) reactions, by analysing the difference in the number of neutrons emitted per reaction. The use of a time correlation analysis of the signals can determine the number of neutron pairs emitted by the contaminant (classical neutron coincidence counting) or even the number of higher order coincidences, such as triplets (counting of neutron multiplicities). Since the (α,n) reaction produces only one neutron, coincidences can only come from fission, thereby providing information independent of the chemical form.

Unlike measurements by gamma spectrometry, it is not possible to precisely identify the emitting isotope by knowing the detection energy as neutrons are most often generated with broad, continuous and non-differentiable energy spectra around 2 MeV (IAEA, 2001).

Precise interpretation of the results therefore requires knowledge of the isotopic composition of the contaminant, either by the traceability of the object (reference spectrum) or by a specific gamma

---

[14]   Further information available here: http://www.ortec-online.com/products/nuclear-security-and-safeguards/neutron-fission-systems/fission-meter

spectrometry measurement. Failing this, only an overall assessment representing all the potential emitting isotopes will be available.

Although less widespread than gamma spectrometry for the characterisation of radioactive waste, passive neutron measurement, particularly in its variant of coincidence counting, is still commonly used. The whole characterisation of the chosen measurement instrument is usually conducted considering standard neutron sources (^{241}Am-Be and ^{252}Cf), as well as numerically with the MCNPX code.

Table 4: Spontaneous neutron emission for some radionuclides of interest (Ensslin et al., 1998).

Radionuclide	Mean neutron multiplicity	Neutron yield (n s^{-1} g^{-1})
^{232}U	1.71	1.3
^{233}U	1.76	8.60×10^{-4}
^{234}U	1.81	5.02×10^{-3}
^{235}U	1.86	2.99×10^{-4}
^{236}U	1.91	5.49×10^{-3}
^{238}U	2.01	1.36×10^{-2}
^{238}Pu	2.21	2.59×10^{3}
^{239}Pu	2.16	2.18×10^{-2}
^{240}Pu	2.16	1.02×10^{3}
^{241}Pu	2.25	0.05
^{242}Pu	2.15	1.72×10^{3}
^{241}Am	3.22	1.18
^{242}Cm	2.54	2.10×10^{7}
^{244}Cm	2.72	1.08×10^{7}

Table 5: Summary of (α,n) yields for some radionuclides of interest (Ensslin et al., 1998).

Radionuclide	Mean alpha energy (MeV)	Alpha yield (α s^{-1} g^{-1})	Neutron yield in UO$_2$/PuO$_2$ (n s^{-1} g^{-1})	Neutron yield in UF$_6$/PuF$_4$ (n s^{-1} g^{-1})
^{232}U	5.3	8.0×10^{11}	1.49×10^{4}	2.6×10^{6}
^{233}U	4.8	3.5×10^{8}	4.8	7.0×10^{2}
^{234}U	4.8	2.3×10^{8}	3.0	5.8×10^{2}
^{235}U	4.4	7.9×10^{4}	7.1×10^{-4}	0.08
^{236}U	4.5	2.3×10^{6}	2.4×10^{-2}	2.9
^{238}U	4.2	1.2×10^{4}	8.3×10^{-5}	0.028
^{238}Pu	5.5	6.4×10^{11}	1.34×10^{4}	2.2×10^{6}
^{239}Pu	5.2	2.3×10^{9}	38.1	5.6×10^{3}
^{240}Pu	5.2	8.4×10^{9}	1.41×10^{2}	2.1×10^{4}
^{241}Pu	4.9	9.4×10^{7}	1.3	1.7×10^{2}
^{242}Pu	4.9	1.4×10^{8}	2.0	2.7×10^{2}
^{241}Am	5.5	1.3×10^{11}	2.69×10^{3}	---
^{242}Cm	6.1	1.2×10^{14}	3.76×10^{6}	---
^{244}Cm	5.8	3.0×10^{12}	7.73×10^{4}	---

Table 6: Data on (α,n) neutron yield and mean energy for light elements (Ensslin et al., 1998).

Target*	Neutron yield per each ^{239}Pu alpha	Mean neutron energy (MeV)
Li	$(113 \pm 25) \times 10^{-8}$	0.3
Be	$(65 \pm 5) \times 10^{-6}$	4.2
B	$(175 \pm 4) \times 10^{-7}$	2.9
C	$(78 \pm 4) \times 10^{-9}$	4.4
O	$(59 \pm 2) \times 10^{-9}$	1.9
F	$(59 \pm 6) \times 10^{-7}$	1.2
Na	$(11 \pm 5) \times 10^{-7}$	---
Mg	$(89 \pm 2) \times 10^{-8}$	2.7
Al	$(41 \pm 1) \times 10^{-8}$	1.0
Si	$(76 \pm 3) \times 10^{-9}$	1.2
Cl	$(7 \pm 4) \times 10^{-8}$	---

*: with natural isotopic concentration

6   Laser induced breakdown spectroscopy

Laser induced breakdown spectroscopy or LIBS is essentially considered as a non-destructive (or minimally-destructive) assay method fully based on the fundamental principle of the ablation of a small amount of sample (10^{-12} to 10^{-9} grams) by focusing a highly energetic laser pulse onto a given surface point (Radziemski & Cremers, 2006). The ablated material then forms a micro-plasma, which almost immediately emits light photons at characteristic wavelengths depending on the elemental composition of the sample. It is hence a very rapid and versatile technique that can, in principle, detect all kind of materials, including impurities, limited only by the power of the laser and the detection performances of the spectrograph sensor. In addition, its wide range of applications is largely driven by its capability with virtually no sample preparation and extremely low detection limit. A typical LIBS setup is shown schematically in Figure 10.
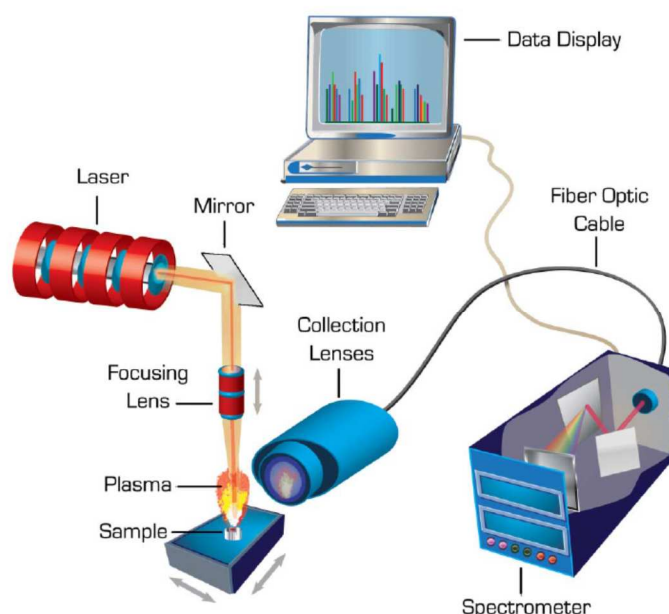

Figure 10: Schematic diagram of a typical LIBS setup, taken from Bol'shakov et al. (2010).

In the case of nuclear facilities, subject to a decommissioning programme, the chosen measurement instrument does not need to be in direct contact with the sample, allowing standoff analysis at distances up to several dozen of meters via optical fibers (Cremers et al., 1995). Another LIBS advantage is its ability to depth profile the sample by repeatedly discharging the laser beam on the same position, by effectively going into more and more depth with each shot. Being exclusively an elemental analysis technique it has also demonstrated its ability to provide a positive identification of fission products, actinides, and activated corrosion products has in many nuclear materials (Fichet et al., 1999; Lang et al., 2018; Martin et al., 2012; Williams & Phongikaroon, 2017). However, at least up till now, this technique is not in common use in the nuclear industry.

7 Radiation cameras

Radiation cameras may provide an optimal solution for in-situ radiological characterisation of nuclear facilities subject to a decommissioning programme. Their associated information regarding the relative intensity of the ionizing radiation being measured (i.e. a sort of colour map display) is directly superimposed on the real view of the scene under study, normally taken by a visible camera. Hence, they allow for the localisation of radioactive objects or hotspots from greater distances than conventional instruments (see Section 2), thus significantly reducing the radiation dose received by operators in line with the well-known ALARA[15] principle.

7.1 Gamma cameras

Based on the measurement principle used, gamma cameras can be classified into three categories: pinhole, coded aperture and Compton gamma. In what follows, we introduce the main concepts of each one of these techniques.

7.1.1 Pinhole technique

A pinhole photographic camera, also known as "dark chamber", is a simple optical imaging device in the shape of a light-opaque box (see Figure 11). In one of its sides is a small aperture through which the light coming from an outside object is projected as an inverted image on the opposite side inside the box.

Initially, the pinhole camera was, in fact, a room where the image was projected onto one of the walls through an opening in the opposite wall (Renner, 1999). It was used to observe solar eclipses and to examine the laws of projection. It later became a portable instrument, which was perfected with a converging lens. Instruments of this kind were often used as drawing aids and, at the dawn of photographic history, they formed the basis for the construction of the camera. During the mid-20th century scientists discovered that this technique could also be used to photograph X- and γ-rays.

While the first photograph taken with a pinhole camera was the work of Scottish scientist Sir David Brewster back in 1850, the technique became more established in photography during the late 19th

---

[15] As Low As Reasonably Achievable. Justification of radiation exposures, optimisation of radiation protection and application of individual dose limits are the three ALARA principles. The International Commission on Radiological Protection, in its Publication 103 (ICRP, 2007), states that: "*the likelihood of incurring exposures, the number of people exposed, as well as the magnitude of their individual doses should be kept as low as reasonably achievable taking into account economic and societal factors*".

century, when it was noted for the soft outlines it produced, as opposed to lenses generating perfect, sharp images. The pinhole camera was later abandoned and it was not until the end of the 1960s that several artists began using it again in their experiments, thus awakening renewed interest in this simple photographic apparatus which endures until now.
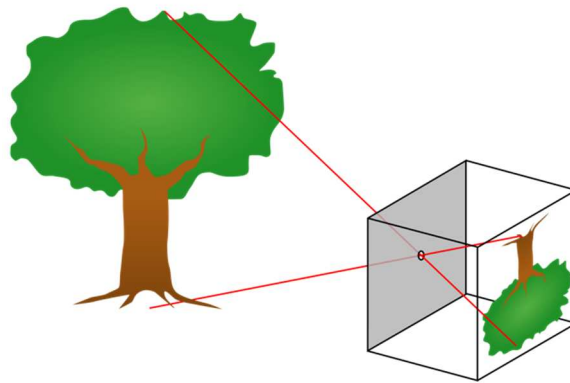
Figure 11: Pinhole camera model (source: Wikipedia).

The image in the pinhole camera is created on the basis of the rectilinear propagation of light (see Figure 11). Each point on the surface of an illuminated object reflects rays of light in all directions. The pinhole lets through a certain number of these rays which continue on their course until they meet the projection plane where they produce a reverse image of the object. Thus the point is not reproduced as a point, but as a small disc, resulting in an image which is slightly out of focus. This description would suggest that the smaller the hole, the sharper the image. However, light is essentially a wave phenomenon and, therefore, as soon as the dimensions of the opening are commensurable with the dimensions of the light wavelength, diffraction occurs.

In other words, if the hole is too small, the image will be out of focus. The calculations for the optimal diameter of the hole in order to achieve the sharpest possible image were first proposed by Josef Petzval (Renner, 1999), and later perfected by Lord Rayleigh (1891).

Images created by a pinhole camera have certain characteristics hardly available in classical lens photography. Since the process entails a central projection, the images in the pinhole camera are rendered in ideal perspective. Another special characteristic is the infinite depth of field which, in a single photograph, allows objects to be captured with equal sharpness whether they are very close up or far away. The pinhole camera takes in an extremely wide angle. The rays of light, however, take much longer to reach the edges of the negative than the centre, thus the picture is less exposed along the edges and therefore darkens. However, its major disadvantage is the lower amount of light allowed through the small aperture, which complicates and sometimes prevents the localisation of moving subjects.

An earlier attempt to develop a portable gamma camera based on the pinhole technique was carried out in the 1990s by CEA (Gal et al., 2001). The outcome of this effort was the CARTOGAM instrument (see Figure 12), which has been widely commercialized by CANBERRA during the last decade. This instrument is a mature technology combining an inverted double-cone collimator (i.e.

two right circular cones placed apex-to-apex) to be used as a single pinhole aperture, a CsI/Tl (thallium doped caesium iodide) scintillation crystal, a multi-channel image intensifier, and a CCD camera. With the exception of the pinhole aperture, the whole instrument is fully shielded against background radiation. This poses several restrictions from a practical point of view.
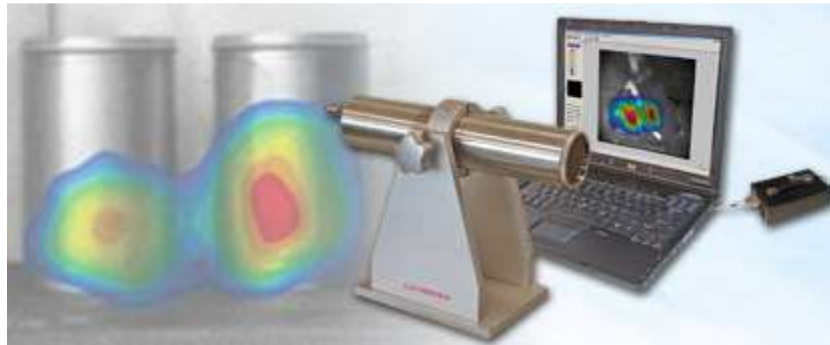
Figure 12: The CARTOGAM gamma camera.

Although considerable progress was made on pinhole gamma cameras, when using these instruments only a very small fraction (less than 0.1%) of the incident γ-rays is transmitted to the detector plane. This fraction can be incremented only by increasing the diameter of the pinhole, thus significantly degrading the spatial resolution of the gamma images obtained. In order to improve the sensitivity and the overall signal-to-noise ratio of the radiation images obtained, the implementation of a coded aperture technique was first tested by the Kurchatov Institute (Ivanov et al., 1999) and then by CEA (Gal et al., 2006).

7.1.2 Coded-aperture technique

The idea of adopting an imaging system based on the coded aperture mask (i.e. a front-end collimator with several pinholes defined by a given rank and thickness in mm) was initially proposed in 1968 by Dicke and Ables, independently. The original motivation was to preserve many of the properties of the pinhole model, like its high angular resolution, while significantly improving the signal-to-noise ratio of the acquired images, proportionally to the sum of the open areas of all the pinholes constituting the coded aperture mask (Caroli et al., 1987). This technique has played a crucial role in astronomy to help resolve the origin of γ-ray bursts from distant galaxies (Vedrenne & Atteia, 2009).

For an accurate localisation of a given radioactive source, a coded aperture mask based on the well-known *Modified Uniformly Redundant Array* or *MURA* (Gottesman & Fenimore, 1989) is placed in front of the pixelated detector, as illustrated in Figure 13. The photon beam coming from the source is modulated by the coded aperture mask and projected on the pixelated detector surface as a shadow image, carrying the coded information of the radioactive source. To obtain the position of the source with respect to the γ-camera field-of-view, we implemented the same reconstruction technique described by Gottesman & Fenimore.
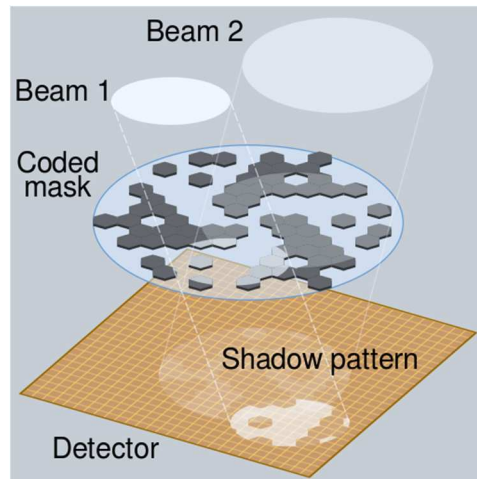
Figure 13: Principle of operation of a MURA coded aperture mask (source: Wikipedia).

As explained by Braga et al. (1991), an important limitation of such a reconstruction technique is the systematics arising from the non-uniform detector spatial response. Moreover, in the correlation process, any variation in the background level measured by different segments of the detector plane can affect the estimates of source intensities. A solution to this problem is to observe the source field in alternate measurements: the mask pattern can be inverted by a 90° rotation. Such rotation creates an anti-mask of the original pattern, except for the central element. This provides an anti-mask measurement without additional weight and complex mechanical manipulations. By performing alternate measurements with a mask and with an anti-mask for equal time durations, the systematic effects are eliminated. The interested reader is referred to Braga et al. (1991) for a detailed explanation of how the anti-mask method works.

CANBERRA has recently developed an ultra-portable and compact gamma camera, called iPIX (Figure 14), in the framework of a partnership agreement with CEA, whose main features and performances have been extensively studied by Amgarou et al. (2016). The system is based on a 1 mm-thick CdTe detector directly bump-bonded to a Timepix chip (Llopart et al., 2007), a pixelated CMOS ASIC developed by CERN consisting of 256 × 256 square pixels with 55 µm side 70 providing a global detection area of ~14 × 14 mm².
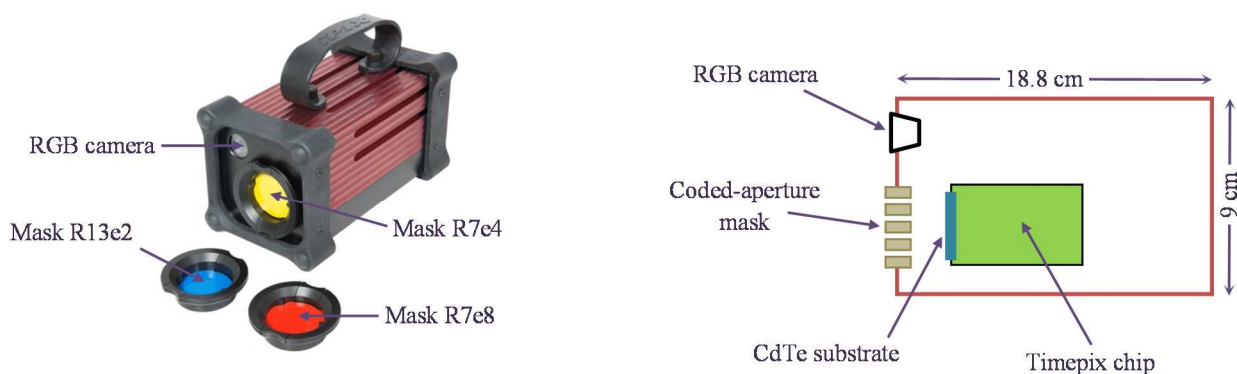
Figure 14: The iPIX gamma imager (left), together with a cross-section not to scale (right) showing its mains components and relevant dimensions (Amgarou et al., 2016).

7.1.3 Compton technique

Cameras based on Compton scattering imaging (Du et al., 2001; Frandes et al., 2016) considers the inelastic photon scattering theory to reconstruct the location of radioactive sources. They typically consist of two parallel and energy sensitive detectors (see Figure 15). When an incoming gamma photon hits the camera, it undergoes Compton scattering in the first detector, called scatter detector, and photoelectric absorption in the second one, called absorber detector. Let E_1 and E_2 be the energies of the recoil electron and of the scattered photon, respectively. By quoting the positions of each interaction and applying the classical laws of conservation of energy and momentum in physics, the scattering angle θ has the following relationship:

$$\cos\theta = 1 - m_e c^2 \left(\frac{1}{E_2} - \frac{1}{E_1 + E_2} \right)$$

being m_e the electron rest mass and c the speed of light.

The primary photon origin can thus be constrained to the surface of a back-projected cone, called the *Compton cone*, spanned by θ with its apex given by the primary interaction position in the scatter detector. From the intersection of different Compton cones, inferred from subsequent photon interactions originating from the same source, the location of this source can be determined.
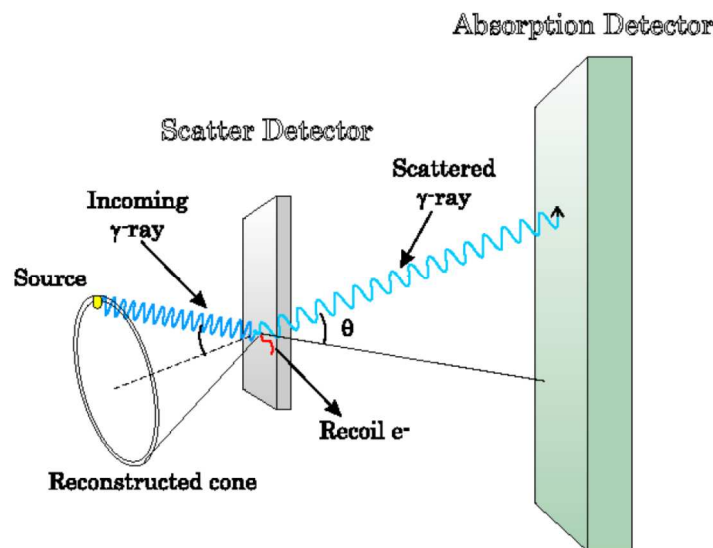
Figure 15: Basic Compton camera concept, taken from Nurdan et al. (2015).

When compared to the coded-aperture technique, Compton gamma cameras present an optimal field-of-view (up to 360°) and a high energy resolu tion (~1% for the [137]Cs 662 keV γ-rays). However, they have a very limited angular resolution (10°− 30°), they cannot be applied for γ-rays below 250 keV and they are less sensitive, as only a small portion of photons are absorbed after the Compton scattering.

7.2 Alpha cameras

Although α-particles are usually hard to measure with conventional detectors due to their short range in air[16], the remote and safe localisation of materials or surfaces contaminated with this kind of radiation is possible based on the ionization-induced fluorescence of airborne molecules. In fact, after depositing their energy in a small layer of air, monochromatic ultraviolet lights are emitted because of the presence of nitrogen.

As illustrated in Figure 16, the strongest emissions by this process occur in the 315.9 nm, 337.1 nm and 357.7 nm wavelengths. This radiation has a very long range in air, allowing the direct visualisation of the location of the corresponding pure alpha sources, with the help of any of the commercially available optical instruments, preferably with an optimum spectral response in the UV-Visible range of interest (i.e., 300 – 750 nm) and appropriate light filters to easily retrieve both pieces of information. Furthermore, such a measurement can also be done through translucent materials and under strong beta and gamma environments, which are not able to generate as much localized fluorescence as in the case of α-particles.

This technique has been widely tested in realistic fields, with encouraging results (Lamadie et al., 2005), and it has the potential to evolve into an industry-standard procedure in the near future. Figure 17 shows how an alpha camera has been successfully applied to locate the surface contamination inside a glovebox of the ATALANTE facility at the CEA Marcoule site, used for the production of powder mixtures and the metallographic preparation of sintered pellets (cutting, coating and polishing). The air inside the glovebox was previously enriched with nitrogen to enhance the measurement.
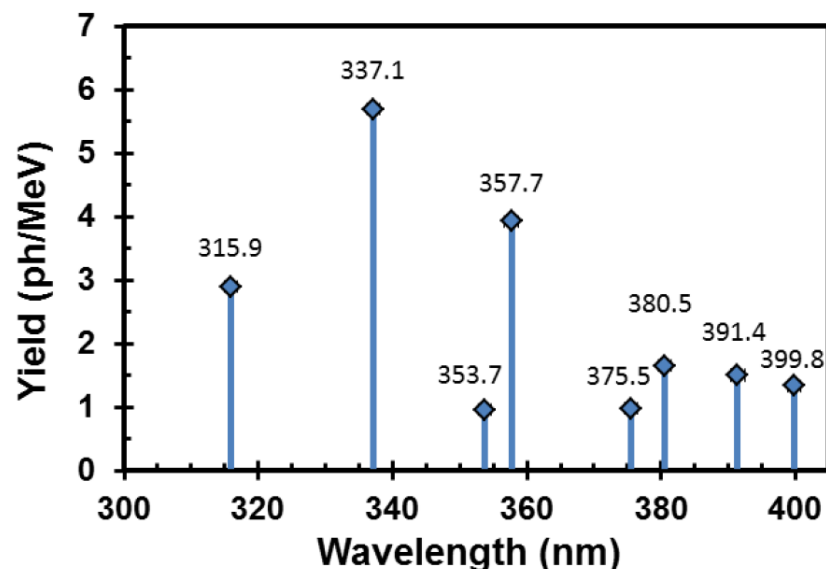
Figure 16: Airborne nitrogen fluorescence yield at sea level for the principle emission peaks in the UV (adapted from Harrison et al., 2015).

---

[16] For example, the range in air of 5.5 MeV α-particles emitted by [238]Pu is ~4 cm.
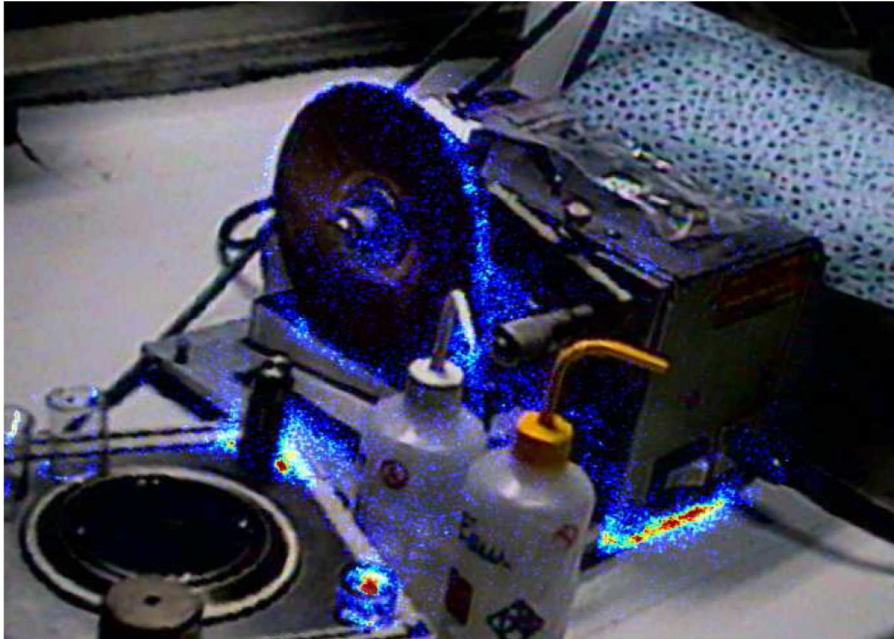
Figure 17: Localisation by means of an alpha camera of the plutonium contamination inside a glovebox of the ATALANTE facility at the CEA Marcoule site.

7.3   Neutron cameras

Because of the ability of neutrons to penetrate objects that are opaque to gamma radiation, the corresponding imaging may be a valuable asset as a non-destructive technique during the dismantling and clean-up of nuclear facilities.

In principle, neutron imaging can also be performed based on both the pinhole and coded-aperture techniques described above (Vanier, 2006; Cieślak et al., 2016). The difference with respect to gamma cameras is the type of materials used for shielding (e.g. lead or tungsten for γ-rays and borated polyethylene for neutrons). In addition, neutrons may undergo proton recoil scattering that can provide analogous directional information, as in the case of the Compton technique, which only applies to photons. However, the mathematical expression for the neutron scattering angle is quite different and it is calculated by kinematics from the energy E_p deposited in the first segmented (or position-sensitive) detector by the recoil proton and the remaining scattered neutron energy, E_{ns}, which can be measured by the time-of-flight method to the second thick detector, as follows:

$$\tan \theta = \sqrt{E_p / E_{ns}}$$

Several prototypes have been recently developed by independent research units for several applications related to the radiation protection of workers, assurance of nuclear non-proliferation safeguards and homeland security, especially the detection of illicit traffic of radioactive materials (Forman et al., 2003; Hausladen et al., 2013; Makowska et al., 2017; Weinfurther et al., 2018). However, the challenge for the initial characterisation of nuclear facilities subject to a decommissioning programme, remains to design neutron cameras that are as compact and robust as possible, so they can be used in constrained environments while remaining sufficiently sensitive

to neutrons and optimizing the angular resolution. Potentially, a good compromise in this aspect may be the one proposed by Whitney et al. (2015), see Figure 18.

Figure 18: The CLYC RadCam-2 system (Whitney et al., 2015).

8   Conclusions

This deliverable D5.1 contains a description of the main non-destructive techniques used for in-situ radiological characterisation of nuclear facilities subject to a decommissioning programme. The document is focused on constrained environments in terms of radioactivity (medium or high radioactivity), under difficult accessibility conditions and/or in underwater interventions. It hence describes instruments usually used for environmental measurements, surface contamination measurements, gamma spectrometry, neutron coincidence measurements, and radiation cameras. Although being exclusively an elemental analysis technique, laser induced breakdown spectroscopy can also be applied to provide complementary and useful information. The main conclusions derived are summarised as follows:

- Environmental radiation measurements

The Geiger-Müller (GM) counter is the most widely used instrument for gross counting, its main advantages are their low price, robustness, a large variety of sizes, and a minimal electronic processing. However, it cannot distinguish between radiation types or energies, it is not able to measure high dose rates and sustained high radiation levels will definitively degrade its detection performance, so it is not recommended for constrained environments.

Air-kerma is universally determined using ionization chambers, which have a good response to photons, and can also tolerate intense radiation fields. However, they cannot discriminate between radiation types and cannot provide the corresponding energy spectrum. Another alternative in the

case of energetic photons is the one based on the energy-compensated silicon diodes, allowing very small-sized detectors to be used for routine surveys in nuclear facilities.

Practically any type of photon detector is able to measure $H^*(10)$, but the preferable one is the proportional counter, which is able to discriminate between radiation types and to provide the corresponding spectrometric information. It also has a small dead time effect and can tolerate high radiation levels. The case of neutrons is much more complex and the available instruments to measure the associated ambient dose equivalent provide satisfactory results only in restricted energy intervals and/or in specific irradiation conditions. Therefore, such instruments must be calibrated under the same experimental configurations or at least considering a representative neutron spectrum.

- Surface contamination measurements

For alpha contamination, gas filled proportional counters or scintillators detectors, with an ultra-thin aluminized Mylar or mica film window, can be used. However, as they must be as close as possible to the object under examination without ever touching it makes direct measurements impractical, except in special and controlled situations. The relatively high penetrating power of β-particles allows increasing the end-window thickness of the above detectors. Nevertheless, beta identification on the basis of energy resolution is virtually impossible and care must be taken (i.e., by varying on the source-to-detector distance or by using an appropriate filter) to well estimate the contribution of gamma radiation.

- Gamma spectrometry

Gamma spectrometry is the start technique for in-situ measurements, as most of the radionuclides emit characteristic X-ray and gamma radiation with specific energies and intensities, making their identification and even their quantification possible. The gamma spectrometers most commonly employed for in-situ measurements are based on inorganic scintillators, such as NaI or LaBr, as well as on high-purity germanium (HPGe), CdTe or CdZnTe semiconductors.

Scintillation detectors can be manufactured in large volumes, but they generally have a poor energy resolution. They are therefore often used for low intensity photon flux measurements with simple gamma spectra. However, since most scintillators have a very fast signal response they can also be used at high counting rates or for coincidence counting.

NaI(Tl) scintillators have a very high detection efficiency and they are available in a wide variety of sizes and geometries. However, their energy resolution is very limited, they do not tolerate high radiation levels, and they are hygroscopic. Consequently, they cannot tolerate exposure to humid environments and they requires the use of a hermetically sealed assembly, which can hinder their detection efficiency for low gamma energies. These detectors provide a stable energy resolution and constant decay time of the light pulses over a wide range of temperatures. They can also be used in underwater applications inside a nuclear fuel storage pool for real-time monitoring.

$LaBr_3$(Ce) scintillators offer improved energy resolution compared to NaI(Tl), a fast emission rate, an excellent temperature tolerance as well as good resistance to intense radiation fields. Although they are currently available in small sizes, they are very appropriate for constrained environments, together with silicon drift detectors (SDD) and silicon photomultipliers (SiPM).

High-purity Germanium (HPGe) detectors are characterised by an excellent energy resolution and they may have large sensitive volumes. Their major drawback is that the crystal must be cooled to liquid nitrogen temperatures, which limits their usefulness in a number of applications, namely in zones with limited accessibility.

The main advantages CdTe and CdZnTe crystals, when compared to the HPGe ones, is their high detection efficiency and its capability to operate at room temperatures. Their energy resolution is not as optimal as that of HPGe, but it is slightly better than that of scintillators. They are also able to carry out in-situ measurements over a wide range of radiation levels. In contrast, they are characterized by a low-energy tailing of the observed peaks in the measured spectrum.

It must be highlighted that semiconductor detectors, in general, are relatively sensitive to performance degradation when exposed to intense radiation fields, namely the ones containing neutrons. Electronic components are also radiation-sensitive, particularly the preamplifiers, which are the first stage in the signal processing chain for most scintillators and semiconductor detectors.

- Neutron coincidence measurements

The main advantage of the passive neutron measurement is its relatively low sensitivity to the density of materials surrounding the radioactive elements. Compared to gamma spectrometry, it is practically insensitive to metallic matrices, making these two techniques quite complementary. However, it is extremely affected by a number of frequently unknown properties, such as the presence in the sample of ^{242}Cm and ^{244}Cm.

The main disadvantage of its basic mode of application (i.e. total neutron counting) is its high sensitivity to the chemical form of the radioactive contaminant, thus it is necessary to discriminate the signal fraction originating from the spontaneous fissions from that resulting from (α,n) reactions. Although this signal discrimination, it is not possible to identify the emitting isotope by knowing the energy of the detected neutron. Precise interpretation of the results therefore requires knowledge of the isotopic composition of the contaminant. Failing this, only an overall assessment representing all the potential emitting isotopes will be available.

- Laser induced breakdown spectroscopy

The major advantage of this minimally-destructive technique is the fact that the chosen measurement instrument does not need to be in direct contact with the sample, allowing standoff analysis of all kind of materials, including impurities, at distances up to several dozen of meters via optical fibers. It also has an extremely low detection limit and it is able to depth profile the sample by repeatedly discharging the laser beam on the same position. However, at least up till now, this technique is not in common use in the nuclear industry.

- Radiation cameras

Radiation cameras allow for the localisation of hotspots from greater distances than conventional instruments thus significantly reducing the radiation dose received by operators.

Gamma cameras based on the pinhole technique provide optimal image quality but they normally have a very small efficiency and the associated shielding poses several restrictions from a practical point of view.

The coded-aperture technique allows to preserve many of the properties of the pinhole gamma cameras, like their high angular resolution, while improving the signal-to-noise ratio of the acquired images without the need for excessive shielding. However, an important limitation of such a reconstruction technique is the systematics arising from the non-uniform detector spatial response. A solution to this problem is to observe the source field in alternate measurements: the mask pattern can be inverted by a 90° rotation.

Cameras based on Compton scattering imaging present an optimal field-of-view and a high energy resolution compared to the coded-aperture technique. However, they have a very limited angular resolution, they cannot be applied for γ-rays below 250 keV and they are less sensitive.

Alpha camera is quite a promising technique. It has been widely tested in realistic fields, with encouraging results and it has the potential to evolve into an industry-standard procedure in the near future. But, right now, is not widely used by the industry.

Several prototypes of neutron cameras have been recently developed for several applications related to the radiation protection of workers, assurance of nuclear non-proliferation safeguards and homeland security. However, the challenge for the D&D processes remains to design neutron cameras more compacts and robust so they can be used in constrained environments while remaining sufficiently sensitive to neutrons and optimizing the angular resolution.

9 Bibliography

Ables, J. G. (1968). *Fourier transform photography: A new method for x-ray astronomy*. Proc. Astron. Soc. Australia, 172.

Amgarou, K., & Lacoste, V. (2010). *Response matrix evaluations of a passive Bonner sphere system used for neutron spectrometry at pulsed, intense and complex mixed fields*. Journal of Instrumentation, 5:P09002.

Amgarou, K., Paradiso, V., Patoz, A., Bonnet, F., Handley, J., Couturier, P., Becker, F., & Menaa, N. (2016). *A comprehensive experimental characterization of the iPIX gamma imager*. Journal of Instrumentation, 11(08):P08012.

Bizarri, G., de Haas, J.T.M, Dorenbos, P., & van Eijk, C.W.E. (2006). *Scintillation properties of Ø 1×1 Inch^3 LaBr$_3$: 5%Ce^{3+} crystal*. IEEE Transactions on Nuclear Science 53(2):615 – 619.

Bramblett, R. L., Ewing, R. I., & Bonner, T. W. (1960). *A new type of neutron spectrometer*. Nuclear Instruments and Methods. 9(1): 1-12.

Braga, J., et al. (1991). *A new mask-antimask coded-aperture telescope for hard x-ray astronomy*. Experimental astronomy, 2(2):101-113.

Baschenko, S.M. (2004). *Remote optical detection of alpha particle sources*. Journal of Radiological Protection, 24, 75-82.

Bol'shakov, A. A., Yoo, J. H., Liu, C., Plumer, J. R., & Russo, R. E. (2010). *Laser-induced breakdown spectroscopy in industrial and security applications*. Applied Optics, 49(13):132-C142.

Cavallini, A., Fraboni, B., Auricchio, N., Caroli, E., Dusi, W., Chirco, P., Morigi, M. P., Zanarini, M., Hage-Ali, M., Siffert, P., & P. Fougeres, P. (2001). *Irradiation-induced defects in CdTe and CdZnTe detectors*. Nuclear Instruments and Methods in Physics Research Section A, 458:392–399.

Caroli, E., et al. (1987). *Coded aperture imaging in x- and gamma-ray astronomy*. Space Science Reviews, 45:349-403.

Cieślak, M. J., Gamage, K. A. A., & Glover, R. (2016). *Coded-aperture imaging systems: Past, present and future development – A review*. Radiation Measurements, 92:59-71.

Cremers, D. A., Barefield, J. E., & Koskelo, A. C. (1995). *Remote Elemental Analysis by Laser-Induced Breakdown Spectroscopy Using a Fiber-Optic Cable*. Applied Spectroscopy, 49(6): 857-860.

Dicke, R. H. (1968). *Scatter-hole cameras for x-rays and gamma rays*. Astrophysical Journal, 153:L101.

Du, Y. F., He, Z., Knoll, G. F., Wehe, D. K., & Li, W. (2001). *Evaluation of a Compton scattering camera using 3-D position sensitive CdZnTe detectors*. Nuclear Instruments and Methods in Physics Research Section A, 457(1):203–211.

Ensslin, N., Harker, W. C., Krick, M. S., Langner, D. G., Pickrell, M. M., & Stewart, J. E. (1998). *Application Guide to Neutron Multiplicity Counting*. Los Alamos National Laboratory, LA-13422-M. Available at:

http://permalink.lanl.gov/object/tr?what=info:lanl-repo/lareport/LA-13422-M

Fichet, P., Mauchien, P., & Moulin C. (1999). *Determination of impurities in uranium and plutonium dioxides by laser-induced breakdown spectroscopy*. Applied Spectroscopy, 53(9):1111-1117.

Forman, L., Vanier, P. E., & Welsh, K. E. (2003). *Fast neutron source detection at long distances using double scatter spectrometry*. Proceedings of the SPIE - Hard X-ray and Gamma-ray Detector Physics V, 5198-33, San Diego. Available at:

https://www.bnl.gov/isd/documents/25565.pdf

Frandes, M., Timar, B., & Lungeanu, D. (2016). *Image Reconstruction Techniques for Compton Scattering Based imaging: An Overview*. Current Medical Imaging Reviews, 12(2):95–105.

Gal, O., Izac, C., Jean, F., Lainé, F., Lévêque, C., & Nguyen, A. (2001). *CARTOGAM - a portable gamma camera for remote localisation of radioactive sources in nuclear facilities*. Nuclear Instruments and Methods in Physics Research A, 460:138-145.

Gal, O., Gmar, M., Ivanov, O. P., Laine, F., Lamadie, F., Le Goaller, Ch., Mahé, C., Manach, E., & Stepanov, V. E. (2006). *Development of a portable gamma camera with coded aperture*. Nuclear Instruments and Methods in Physics Research A, 563(1):233-237.

Gottesman, S. R., & Fenimore, E. E. (1989). New family of binary arrays for coded aperture imaging. Applied Optics, 28:4344-4352.

Harrison, R. K, Martin, J. B., Wiemann, D., Choi, J., & Howell, S. (2015). New radiological material detection technologies for nuclear forensics: remote optical imaging and graphene-based sensors. Sandia National Laboratories, Report SAND2015-7567.

Available at: http://prod.sandia.gov/techlib/access-control.cgi/2015/157567.pdf

Hausladen, P., Newby, J., Liang, F., & Blackston, M. (2013). *A deployable fast-neutron coded-aperture imager for quantifying nuclear material*. Oak Ridge National Laboratory. ORNL/TM-2013/248. Available at: https://info.ornl.gov/sites/publications/Files/Pub44511.pdf

IAEA (2001). *Compendium of neutron spectra and detector responses for radiation protection purposes*. International Atomic Energy Agency, Supplement to Technical Reports Series No. 318. Available at: http://www-pub.iaea.org/MTCD/Publications/PDF/TRS403_scr.pdf

IAEA (2016). *IAEA safety glossary: terminology used in nuclear safety and radiation protection*. International Atomic Energy Agency, Revision of the 2007 edition. Available at: http://www-ns.iaea.org/

IAEA (2017). *In situ analytical characterization of contaminated sites using nuclear spectrometry techniques*. International Atomic Energy Agency, IAEA Analytical Quality in Nuclear Applications Series No. 49, Available at: http://www-pub.iaea.org/books/IAEABooks/12227/In-Situ-Analytical-Characterization-of-Contaminated-Sites-Using-Nuclear-Spectrometry-Techniques

ICRP (1991). *1990 recommendations of the international commission on radiological protection*. International Commission on Radiological Protection, ICRP Publication 60, Annals of the ICRP 21(1-3).

ICRP (1996). *Conversion coefficients for use in radiological protection against external radiation*. International Commission on Radiological Protection, ICRP Publication 74, Annals of the ICRP 26(3-4).

ICRP (2007). *2007 recommendations of the international commission on radiological protection*. International Commission on Radiological Protection, ICRP Publication 103, Annals of the ICRP, 37(2-4).

ICRP (2012). *Statement on tissue reactions / Early and late effects of radiation in normal tissues and organs – threshold doses for tissue reactions in a radiation protection context*. International Commission on Radiological Protection, ICRP Publication 118, Annals of the ICRP, 41(1-2).

ICRU (1985). *Determination of dose equivalents resulting from external radiation sources*. International Commission on Radiation Units and Measurements, ICRU Report 39.

ICRU (1993). *Quantities and Units in Radiation Protection Dosimetry*. International Commission on Radiation Units and Measurements, ICRU Report 51.

ISO (2016a). *Measurement of radioactivity – Measurement and evaluation of surface contamination – Part 1: General principles*. International Organization for Standardization, ISO 7503-1:2016.

ISO (2016b). *Measurement of radioactivity − Measurement and evaluation of surface contamination − Part 2: Test method using wipe-test samples*. International Organization for Standardization, ISO 7503-2:2016.

ISO (2016c). *Measurement of radioactivity − Measurement and evaluation of surface contamination − Part 3: Apparatus calibration*. International Organization for Standardization, ISO 7503-3:2016.

Ivanov, O. P., Sudarkin, A. N., Stepanov, V. E., & Urutskoev, L.I. (1999). *Portable X-ray and gamma-ray imager with coded mask: performance characteristics and methods of image reconstruction*. Nuclear Instruments and Methods in Physics Research A, 422(1):729-734.

Knoll, G. F. (2010). *Radiation Detection and Measurement*. John Wiley & Sons, Fourth Edition.

Lamadie, F., Delmas, F., Mahé, C., Gironès, P., Le Goaller, C., Costes, J.R. (2005). *Remote alpha imaging in nuclear installations: New results and prospects*. IEEE Transactions on Nuclear Science, 52, 3035-3039.

Lang, A., Engelberg, D., Smith, N. T., Trivedi, D., Horsfall, O., Banford, A., Martin, P. A., Coffey, P., Bower, W. R., Walther, C., Weiß, M., Bosco, H., Jenkins, A., & Law, G. T.W. (2018). *Analysis of contaminated nuclear plant steel by laser-induced breakdown spectroscopy*. Journal of Hazardous Materials, 345:114-122.

Leskinen, A., Fichet, P., Siitari-Kauppi, M., & Goutelard, F. (2013). *Digital autoradiography (DA) in quantification of trace level beta emitters on concrete*. Journal of Radioanalytical and Nuclear Chemistry, 298, 153-161.

Llopart, X., Ballabriga, R., Campbell, M., Tlustos, L., & Wong, W. (2007). *MEDIPIX, a 65k programmable pixel readout chip for arrival time, energy and/or photon counting measurements*, Nuclear Instruments and Methods in Physics Research A, 581:485-494.

Makowska, M. G., Walfort, B., Zeller, A., Grünzweig, C., & Bücherl T (2017). *Performance of the commercial PP/ZnS:Cu and PP/ZnS:Ag scintillation screens for fast neutron imaging*. Journal of Imaging, 3:60.

Martin, M., Allman, S., Brice, D., Martin, R., & Andre, N. (2012). *Exploring laser-induced breakdown spectroscopy for nuclear materials analysis and in-situ applications*. Spectrochimica Acta Part B, 74–75:177-183.

Mikami, S., Maeyama, T., Hoshide, Y., Sakamoto, R., Sato, S., Okuda, N., Sato, T., Takemiya, H., & Saito, K. (2015). *The air dose rate around the Fukushima Dai-ichi Nuclear Power Plant: its spatial characteristics and temporal changes until December 2012*. Journal of Environmental Radioactivity, 139, 250-259.

Moszynski, M.; Nassalski, A.; Syntfeld-Kazuch, A.; Szczensniak, T.; Czarnacki, W.; Wolski, D.; Pausch, G.; Stein, J. (2006). *Temperature dependences of $LaBr_3(Ce)$, $LaCl_3(Ce)$ and NaI(Tl) scintillators*. Nuclear Instruments and Methods in Physics Research Section A, 588(2), 739-751.

Normand, S.; Iltis, A.; Bernard, F.; Domenech, T.; Delacour, P. (2006). *Resistance to γ irradiation of LaBr3:Ce and LaCl3:Ce single crystals.* Nuclear Instruments and Methods in Physics Research Section A, 572(2), 754-759.

Nurdan, T. C., Nurdan, K., Brill, A B., & Walenta, A. H. (2015). Design criteria for a high energy Compton Camera and possible application to targeted cancer therapy. Journal of Instrumentation, 10:C07018.

Ören, Ü., Herrnsdorf, L., Gunnarsson, M., Mattsson, S., Rääf, C. L. (2016). *Can an energy-compensated solid-state x-ray detector be used for radiation protection applications at higher photon energies?* Radiation Protection Dosimetry, 169(1-4):292–296.

Park, S. H., Ha, J. H., Lee, J. H., Kim, H. S., Cho, Y. H., Cheon, S. D., & Hong, D. G. (2010). *Effect of temperature on the performance of a CZT radiation detector*. Journal of the Korean Physical Society, 56(4):1079-1082.

Pelowitz, D. B. (2011). *MCNPX^{TM} user's manual, version 2.7.0*. Los Alamos National Laboratory, LA-CP-11-00438.

Pérot, B., Jallu, F., Passard, C., Gueton, O., Allinei, P. G., Loubet, L., Estre, N., Simon, E., Carasco, C., Roure, C., Boucher, L., Lamotte, H., Comte, J., Bertaux, M., Lyoussi, A., Fichet, P., & Carrel, F. (2018). *The characterization of radioactive waste: a critical review of techniques implemented or under development at CEA, France*. EPJ Nuclear Sciences and Technologies, 4, 3.

Pullia, A., Zocca, F., & Cattadori, C. (2005). *Single-transistor option for high-resolution γ-ray spectroscopy in hostile environments*. Nuclear Science Symposium Conference Record, 8986075.

Radziemski, L. J.; Cremers, D. A. (2006). *Handbook of laser-induced breakdown spectroscopy*. New York: John Wiley.

Reilly, D., Ensslin, N., & Smith, H. Jr (1991). *Passive non-destructive assay of nuclear materials*. Los Alamos National Laboratory. NUREG/CR-5550/LA-UR-90-732. Available at:

http://www.lanl.gov/orgs/n/n1/FMTTD/neut_mc/pdfs/LA_UR_90_0732.pdf

Renner, E. (1999). *Pinhole Photography*. Rediscovering a Historic Technique. Boston and London: Focal Press, 2nd edition.

Strutt Lord Rayleigh, J. W. (1891). *Some applications of photography*. Nature, 44 (1133):249-254.

Tahmasebi Birgani, M. J., Seif, F., Chegeni, N., & Bayatiani, M. R. (2012). *Determination of the effective atomic and mass numbers for mixture and compound materials in high energy photon interactions*. Journal of Radioanalytical and Nuclear Chemistry, 292:1367–1370.

Takeda, S., Ichinohe, Y., Hagino, K., Odaka, H., Yuasa, T., IkeIshikawa, S., Fukuyama, T., Saito, S., Sato, T., Sato, G., Watanabe, S., Kokubun, M., Takahashi, T., Yamaguchi, M., Tajima, H., Tanaka, T., Nakazawa, K., Fukazawa, Y., & Nakano, T. (2012). *Applications and Imaging Techniques of a Si/CdTe Compton Gamma-Ray Camera*. Physics Procedia, 37, 859-866.

Tsoulfanidis, N., & Lansberger, S. (2015). *Measurement and Detection of Radiation*. CRC Press, 4th edition.

Vanier, P. E. (2006). *Analogies between neutron and gamma-ray imaging*. Brookhaven National Laboratory. BNL-76974-2006-CP. Available at:

https://pdfs.semanticscholar.org/90f8/862d140b769b3fdf878d21e4168ccb3d07ca.pdf

Vedrenne, G., & Atteia, J.-L. (2009). *Gamma-Ray Bursts: The brightest explosions in the Universe*. Springer/Praxis Books.

Weinfurther, K., Mattingly, J., Brubaker, E., & Steele, J. (2018). *Model-based design evaluation of a compact, high-efficiency neutron scatter camera*. Nuclear Instruments and Methods in Physics Research Section A, 883(1):115-135.

Whitney, C. M., Soundara-Pandian, L., Johnson, E. B., Vogel, S., Vinci, B., Squillante, M., Glodo, J., & Christian, J. F. (2015). *Gamma–neutron imaging system utilizing pulse shape discrimination with CLYC*. Nuclear Instruments and Methods in Physics Research A, 784:346–351.

Williams, A., & Phongikaroon, S. (2017). *Laser-induced breakdown spectroscopy (LIBS) in a novel molten salt aerosol system*. Applied Spectroscopy, 71(4):744-749.

Woolf, R.S., Phlips, B.F., Hutcheson, A.L., & Wulf, E.A. (2015). *Fast-neutron, coded-aperture imager*. Nuclear Instruments and Methods in Physics Research Section A, 784, 398-404.

Appendix A: Radiation protection basics

Radiation protection essentially aims at controlling exposure to ionizing radiation[17] to prevent acute damage and reduce the risk of long-term effects in humans to acceptable levels. For this purpose, the International Commission on Radiation Protection has defined, in its Publication 60 (ICRP, 1991), a radiation protection system, which still prevails today, that allows the evaluation of the extent of exposure to ionizing radiation from intakes of radionuclides as well as from both whole and partial body external irradiation. This system has the following three objectives:

- The characterisation of the radiation fields and their interactions with matter from physical and measurable quantities; the so-called **primary quantities**.

- The definition of **protection quantities** that play a central role for estimating the stochastic health risk due to long-term radiation exposure at low doses, and from which legal limits to the public and occupational radiation exposure can be created.

- The establishment of a series of **operational quantities**, to be used in practical controls of external radiation fields, as protection quantities are not directly measurable.

A-1. Primary quantities

The three primary quantities most widely used in radiation protection are: **fluence**, **kerma** and **absorbed dose**. All of them are scalar physical quantities that characterise the radiation field and their interaction with matter.

a. Fluence

Fluence, Φ, is defined by the number of particles dN traversing a sphere, divided by the cross-sectional area dS of this latter. That is:

$$\Phi = \frac{dN}{dS} \tag{A-1}$$

Its SI unit is cm^{-2} and when divided by the exposure time, it is known as fluence rate or $\dot{\Phi}$ with the general unit of cm^{-2} s^{-1}.

The definition of such sphere allows the corresponding cross-sectional area, perpendicular to the direction of each incoming particle, to be accounted for. Therefore, fluence does not depend on the direction distribution of the incoming particles.

It is also very common in dosimetric calculations to express fluence in terms of the lengths of the particle trajectories in the considered medium:

$$\Phi = \frac{\Sigma dl}{dV} \tag{A-2}$$

where Σdl is the sum of all the lengths of particle trajectories in the volume dV of the considered sphere.

---

[17] Ionizing radiation refers to both charged particles (e.g. electrons or protons) and neutral particles (e.g. photons or neutrons) that produce ionization in a medium. This ionization, in the case of neutral particles, is an indirect process, since they first produce charged particles, which in turn transfer energy to the surrounding atoms.

b. Kerma

Kerma, **K**, is the sum of the initial kinetic energies per unit mass of the charged particles that are released by indirectly ionizing or uncharged radiation, such as photons and neutrons, in a sample of matter. The SI unit of kerma is one joule per kilogram (J kg^{-1}) and its special name is Gray (Gy). When divided by the exposure time, it is known as kerma rate or $\dot{K}$, with the most common unit being mGy/h.

Kerma depends only on the local interactions of the incident uncharged radiation, whereas the absorbed dose also considers all the secondary charged particles, originally released in the surrounding medium, that are able to reach the considered volume, depositing energy in it.

c. Absorbed dose

The absorbed dose, or simply "dose", **D**, is the mean energy imparted by ionizing radiation to matter per unit mass of the matter. Similar to kerma, its SI unit is the Gray (Gy), and when divided by the exposure time, it is known as dose rate or $\dot{D}$, with the most common unit being mGy/h.

The definition of absorbed dose has the scientific rigor required for a basic physical quantity, as it implicitly takes into account the different radiation interactions with matter inside and outside the specified volume. It does not, however, consider the atomic structure of matter and the stochastic nature of the radiation interactions at a microscopic level.

A-2. Protection quantities

The major drawback of the primary quantities is their inadequacy to estimate the ionizing radiation risk due to induced stochastic health effects. This risk depends both on the type of organ or tissue affected and on the type of ionizing radiation. For that reason, additional quantities have been defined to take into account variations in the biological effectiveness of each ionizing radiation, as well as the different sensitivities of human organs and tissues to the same absorbed dose.

a. Equivalent dose

The equivalent dose in a human organ or tissue, H_T, is a radiation-weighted dose quantity that takes into account the type of ionizing radiation as follows:

$$H_T = \sum_R w_R D_{T,R}$$

(A-3)

where $D_{T,R}$ is the is the absorbed dose in the human organ or tissue T by the ionizing radiation R, and w_R is the radiation weighting factor. The sum is performed over all types of radiation involved. The SI unit of the equivalent dose is J/kg^{-1} and has the special name of Sievert (Sv). When divided by the exposure time, it is known as equivalent dose rate or $\dot{H}_T$, with the most common unit being mSv/h.

The Sievert unit is also used for the effective dose, as well as for operational dose quantities (see the following sections), although the meaning of each one of them is not the same. Therefore, care must be taken to ensure that the dosimetric quantity being used is clearly stated.

The values of w_R were defined largely on the basis of the relative biological effectiveness (RBE) of the different types of ionizing radiation, see Table A-1. They are specified in terms of type and, in

the case of neutrons, in terms of energy of radiation, either by incident on the human body or emitted by radionuclides residing in the body:

$$w_R = \begin{cases} 2.5 + 18.2 \times \exp\left(-\frac{\ln^2(E_n)}{6}\right), & E_n < 1 \text{ MeV} \\ 5.0 + 17.0 \times \exp\left(-\frac{\ln^2(2 \times E_n)}{6}\right), & 1 \text{ MeV} \leq E_n \leq 50 \text{ MeV} \\ 2.5 + 3.25 \times \exp\left(-\frac{\ln^2(0.04 \times E_n)}{6}\right), & E_n > 50 \text{ MeV} \end{cases} \qquad \text{(A-4)}$$

b. Effective dose

The notion of effective dose, $\mathbf{E}$, was defined to take into account that the probability of biological effect depends on both the type of ionizing radiation and the irradiated human organ or tissue. It can be calculated as the tissue-weighted sum of the equivalent doses over all organs and tissues of the human body considered to be sensitive to the induction of cancer and/or genetic mutations:

$$\mathbf{E} = \sum_T w_T H_T = \sum_T w_T \sum_R w_R \mathbf{D}_{T,R} \qquad \text{(A-5)}$$

where w_T is the weighting factor for the considered tissue T (with $\sum_T w_T = 1$).

As stated above, the SI unit of the effective dose is the Sievert (Sv), and when divided by the exposure time, it is known as the effective dose rate or $\dot{\mathbf{E}}$, with the most common unit being mSv/h.

The recommended w_T values for different organs and tissues are given in Table A-2. They are based on the latest epidemiological data on cancer induction.

Table A-1: Radiation weighting factors (ICRP, 2007).

Radiation Type	w_R
Photons	1
Electrons	1
Muons	1
Protons	2
Charge pions	2
Alpha particles	20
Fission fragments	20
Heavy ions	20
Neutrons	See Eq. (A-4)

Table A-2: Recommended tissue weighting factors (ICRP, 2007).

Tissue	w_T	$\sum_T w_T$
Bone-marrow (red), colon, lung, stomach	0.12	0.72
Breast, gonads, remainder tissues[18]	0.08	0.08
Bladder, oesophagus, liver, thyroid	0.04	0.16
Bone surface, brain, salivary glands, skin	0.01	0.04
	Total	**1**

A-3. Operational quantities

Neither the effective dose, $\mathbf{E}$, nor the equivalent dose, H_T, are quantities that can be measured in a straightforward manner. For this reason, they cannot be used directly for external radiation monitoring. This circumstance has forced the International Commission on Radiation Units and Measurements, in its Report 39 (ICRU,1985), to introduce operational quantities to be used in both area and individual monitoring of external radiation fields. This allows, in principle, a conservative estimate of the aforementioned protection quantities under nearly all irradiation conditions.

Up to three operational dose quantities, which are intended to be measurable and traceable to pre-established calibration procedures (see Section A-4), are required for each specified task in radiological protection in order to surrogate $\mathbf{E}$ and H_T. These include area monitoring for controlling the radiation in workplaces, and personal dosimetry for the control and diminution of individual exposure. While measurements with an area monitor are preferably performed free in air, personal dosimeters are worn on the body. As a consequence, in a given situation, the radiation field '*seen*' by an area monitor free in air differs from that '*seen*' by a personal dosimeter worn on the body, where the radiation field may be influenced by backscatter and by absorption of radiation into the body itself.

Using the summary in Table A-3, it is not necessary to use the former terms '*strongly penetrating ionizing radiation*' and '*weakly penetrating ionizing radiation*' in specifying the range of application of these operational quantities. The ICRU Report 51 (ICRU, 1993) stated that $H^*(10)$ and $H_p(10)$ are designed for monitoring strongly penetrating ionizing radiation (e.g. photons above 12 keV and neutrons), whereas $H'(0.07,\Omega)$ and $H_p(0.07)$ are applied for monitoring low-penetrating ionizing radiation (e.g. beta particles). Furthermore, $H_p(0.07)$ is also used for monitoring the skin dose from all ionizing radiation. For the special case of controlling the dose to the eye lens, $H'(3,\Omega)$ and $H_p(3)$ are strongly recommended. In fact, the ICRP publication 118 (ICRP, 2012) revised downwards the occupational exposure limits associated to this organ because of recent epidemiological studies that showed a higher incidence of cataracts than expected at low doses (< 0.5 Gy).

---

[18] Such as adrenals, extra-thoracic region, gall bladder, heart, kidneys, lymphatic nodes, muscle, tongue, mucosa, pancreas, prostate, small intestine, spleen, thymus, and uterus/cervix.

The definitions of the three operational quantities are given below.

Table A-3: Operational quantities for external radiation monitoring.

Task	Area Monitoring	Individual monitoring
Control of effective dose	Ambient dose equivalent $H^*(10)$	Personal dose equivalent $H_p(10)$
Control of equivalent dose to skin	Directional dose equivalent $H'(0.07,\Omega)$	Personal dose equivalent $H_p(0.07)$
Control of equivalent dose to eye lens	Directional dose equivalent $H'(3,\Omega)$	Personal dose equivalent $H_p(3)$

a. Ambient dose equivalent

The ambient dose equivalent, $H^*(10)$, is the absorbed dose that would be, by the corresponding expanded[19] and aligned[20] field, at a depth of 10 mm on the radius of an imaginary ICRU sphere (Figure A-1) of 30 cm diameter, 1 g/cm^{-3} mass density and made of a tissue equivalent material[21], located at the point of interest and oriented opposite to the direction of such aligned field. With this definition, $H^*(10)$ should hypothetically estimate the effective dose **E** regardless of the irradiation geometry. When divided by the exposure time, it is known as ambient dose equivalent rate or $\dot{H}^*(10)$.
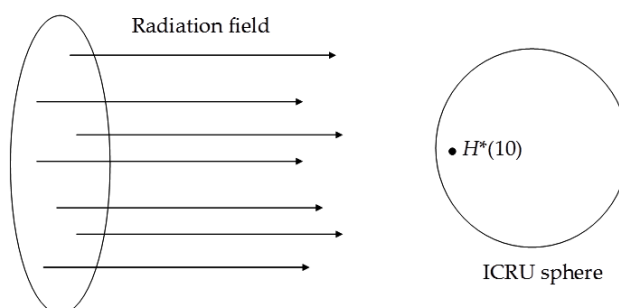
Figure A-1: Concept of ambient dose equivalent *H**(10).
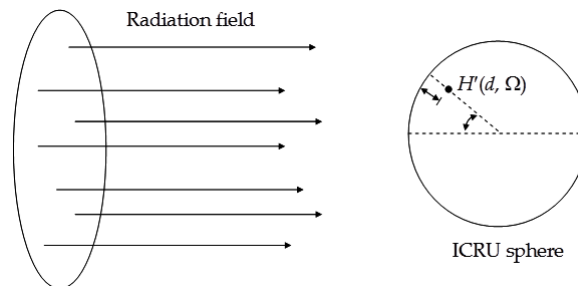
b. Directional dose equivalent

The directional dose equivalent, $H'(d,\Omega)$, at a given point in a radiation field, is the dose equivalent that would be produced by the corresponding expanded field in the ICRU sphere at a depth d, on a radius in a specified direction Ω (see Figure A-2). When divided by the exposure time, it is known as directional dose equivalent rate or $H'(d,\Omega)$.

---

[19] A hypothetical radiation field in which the spectral and the angular fluence have the same value in all points of a sufficiently large volume to ensure a homogeneous exposition.
[20] A hypothetical radiation field in which the fluence is unidirectional.
[21] Chemical composition: 76.2% oxygen + 11.1% carbon + 10.1% hydrogen + 2.6% nitrogen.

For low-penetrating radiation the recommended depth is 0.07 mm and the directional dose equivalent must be $H'(0.07,\Omega)$.

Figure A-2: Concept of directional dose equivalent H'(d,Ω).

c. Personal dose equivalent

The personal dose equivalent, $H_p(d)$, is the dose equivalent in ICRU tissue at a depth d in a human body below the position where an individual dosimeter is worn. When divided by the exposure time, it is known as personal dose equivalent rate or $\dot{H}_p(d)$.

For the assessment of the effective dose, a depth d = 10 mm is recommended, whereas the recommended depth for assessing the equivalent dose to the skin is d = 0.07 mm. As stated above, it has been proposed that a depth of d = 3 mm would be more appropriate to control the equivalent dose to the eye lens.

A-4. Calibration procedures

Calibration of area monitors in terms of $H^*(10)$ and $H'(d,\Omega)$ is performed free in air by determining the appropriate primary quantity (i.e. air kerma for photons, fluence for neutrons and absorbed dose for electrons)[22] and applying the corresponding energy-dependent conversion coefficients given in (ICRP, 1996).

On the opposite, calibration of $H_p(d)$ needs the use of an appropriate personal dosimeter mounted on a slab phantom representing parts of human bodies. To accomplish this objective, the following three phantoms are frequently proposed (see Figure A-3):

- A PMMA cube filled with water to simulate the human torso with external dimensions of 30 cm × 30 cm × 15 cm. All of its walls are 10 mm thick except the front one that must not exceed 2.5 mm thick.

- A PMMA circular cylinder, of 73 mm diameter and 300 mm length, filled with water to simulate a lower human arm or leg. Its lateral wall must be 2.5 mm thick while the corresponding bottom and cover plates are 10 mm thick each.

- A PMMA rod of 19 mm diameter and 300 mm length to simulate a human finger.

---

[22] This is only true in Radiation Protection; however, for medical therapeutic [yo borraría therapeutic y dejaría solo medical, es repetitivo] applications, the absorbed dose (to water) is also used for photons and air kerma for neutrons in order to properly calibrate the quality properties of the planned irradiation beams.

Conversion coefficients relating to the primary (air kerma in the case of photons) and operational quantities have to be calculated assuming vacuum outside of the ICRU sphere and the above phantoms.

Figure A-3: Phantoms representing parts of human bodies (torso, arm and finger).